NRC·CNRC Aerospace

Civil Aviation Alternate Fuels Contrails and Emissions Research – Contrails Analysis

LTR-FRL-2018-0014

A P Brown, M Bastian

Flight Research Laboratory

February 2018

National Research Council Canada | Conseil national de recherches Canada

Canada

Table of Contents

Table of Figures

Figure 15 – plot of $A\partial RH/\partial z^{a}T_S^{b}RH_{ICEce}^{c}$ identified separately for each of the two fuel types, against contrail cross-section data-point age

Figure 16 – plots of CAAFCER & ACCESS II NRC data of FSSP-100 AEIm against atmospheric temperature T_S, RH lapse rate $\partial RH/\partial z$ and relative humidity over $_{ICE}$ RH_{ICECE}.

Figure 17 – plots of log-normal (by 10^8 µg/kg) $A\partial RH/\partial z^{a}T_S^{b}RH_{ICEce}^{c} = \log_{10}$[FSSP AEIm], identifications of contrail spherically-assumed $_{ICE}$-mass, for *each* of the two separate fuel type contrails

Figure 18 – plot of $A\partial RH/\partial z^{a}T_S^{b}RH_{ICEce}^{c}$ identified separately for each of the two fuel types, against contrail cross-section data-point age.

Figure 19 – contrail $_{ICE}$ particle spectra, FSSP-100, in homogenous sections of the contrail, at various contrail lengths:- t*op, left to right*, 15 nm, 18 nm, 22 nm; *bottom, left to right*, 35 nm, 45 nm

Figure 20(a) – contour crossplane plots of contrail FSSP-100 $_{ICE}$ particle spectral MED (43% HEFA contrail, 3rd May 2017), showing size growth in the UJW and sublimation in the TWV regions over increasing contrail length:- t*op, left to right*, 8 nm, 12 nm; *bottom, left to right*, 15 nm, 18 nm.

Figure 20(b) – contour crossplane plots of contrail FSSP-100 $_{ICE}$ particle spectral MED (Jet A1 contrail, 3rd May 2017), showing size growth in the UJW and sublimation in the TWV regions over increasing contrail length:- t*op, left to right*, 123nm, 16 nm; *bottom, left to right*, 19 nm, 22 nm.

Figure 21 – plots of median MED for each contrail cross-sections, plotted against *top left*, contrail age (and along-track spatial changes) and atmospheric parameters, *top right*, T_S, *bottom left*, RH_{ICEce}, *bottom right*, $\partial RH/\partial z$.

Figure 22 – plots of identified power-law parametric variations of contrail cross-section median MED with atmospheric properties, for the two fuel types used on CAAFCER,

Acknowledgement

In preparing the CAAFCER contrails analysis report, the contributions and consultancy of the following are acknowledged:

Mena Salib and Francesco Femia, Air Canada
Fred Ghatala, The Waterfall Group
Jason Olfert, University of Alberta
Renco Beunis and Misha Valk, SkyNRG
Nathalie Gaudet, QETE, DND
Steven Baughcum, The Boeing Company

Abbreviations

ACCESS II	NASA project Alternate Fuel Effects on Contrails & Cruise Emissions, phase II
AEIn	Contrail $_{ICE}$ particle number Apparent Emissions Index[7], number per kg of fuel burned, for $_{ICE}$ particles >0.5µm in size, as measured along the contrail; thus, AEIn might change under microphysical processes, in response to varying background atmospheric conditions, by the NRC CT-133 FSSP-100 probe of ECCC
ATC	Air traffic control
BC	emitted black carbon particles (soot)
CAAFCER	GARDN project *Civil Aviation Alternate Fuel Contrails and Emissions Research*, funded by GARDN and awarded to The Waterfall Group, with enabling In-kind contributions from Air Canada and other consortium members (Sky NRG, University of Alberta, Boeing)
c.f.	*confer/conferatur*, Latin, meaning 'compared with'
CN	Condensation nuclei
CPC	Condensation particle counter
DAS	Data acquisition system
DND	Department of National Defence of Canada
ECCC	Environment and Climate Change Canada
EIm	Emission Index by mass per kg fuel burned
EIn	Number Emission index by number per kg of fuel burned
EI_S	Emissions Index of Soot (#/kg)
FIRNS	FRL inertial reference and navigations system (integrated HG1700 IMU, Novatel GPS and DRP system)
FMS	Flight management system
FSSP-100	Forward scattering spectrometric probe
GARDN	Green Aviation Research & Development Network of the Government of Quebec
GTL	Gas Turbine Laboratory of the NRC Aerospace Research Centre
HAARC	NRC High altitude atmospheric research capability
HEFA	Hydro-processed Esters and Fatty Acids
LOF	line of flight
LVW	Lower viscous wake (wake regime below the TWV)
M	Mach Number
MCT	maximum continuous thrust
MED	Median effective diameter – the spherical $_{ICE}$ particle diameter equating to the 50th percentile of the FSSP-100 cumulative volumetric distribution of the particle size spectrum
MLE	Maximum likelihood estimator

NRC	National Research Council of Canada
N_1	Engine gas generator rotational speed (%)
NMR	Nuclear magnetic resonance measurement of total hydrogen content
nvPM	Non-volatile particulate matter (such as black carbon), namely the residual particles that have not been vapourised by the denuder (maintained at a temperature >300°C)
PM	Particulate matter emissions, i.e. non-volatile and volatile, as counted by the CN 7610 or the CPC 3776 (with denuder in bypass)
P_S	Atmospheric static air pressure
P_T	Atmospheric total air temperature
QAR	Quick access recorder, part of the aircraft flight data recorder
QETE	Quality Engineering Test Establishment of the Department of National Defence
RH	Relative humidity
RH_{ICE}	RH over $_{ICE}$
TGT	Engine turbine gas temperature (°C)
THC	Total hydrogen content
T_S	Static air temperature (°C)
TWV	Trailing wake vortex crossplane flow region
UJW	Upper jet wake; generally the UJW in cross-sectional shape is a '**T**', the lateral being the UJW crown, the vertical being the UJW stem, and the foot being the TWV region.
UTLS	Upper troposphere lower stratosphere
vPM	Volatile particulate matter
WV	Trailing pair of wake $vort_{ICE}$s
[x]	Line-of-flight (LoF) axis direction (upstream is positive), mean LoF is aligned with the contrail mean axial direction
[y]	Lateral direction (to the right is positive, looking upstream)
[z]	Normal direction (upwards is positive)
α_{DP}	α (incidence or angle-of-attack) probe differential pressure

Abstract

In 2017, the Green Aviation Research and Development Network (GARDN) project Civil Aviation Alternate Fuels Contrails and Emissions Research (CAAFCER) was undertaken by a consortium of Air Canada, The Waterfall Group, The University of Alberta, SkyNRG, The Boeing Company and the NRC.

The NRC CT-133 research jet undertook flight measurements of contrail $_{ICE}$ particle size and number, particulate and gaseous emissions from Air Canada A320 series jets in cruise, flying respectively on bulk JetA1 and pre-blended 43% HEFA-biofuel-JetA1 blend. The HEFA was supplied by AltAir of Los Angeles. Air Canada conducted the blend in Montreal. Intertek conducted full ASTM analyses of the fuel blend. Air Canada jets, fueled with the HEFA-blend, departed Montreal Airport for Toronto. The NRC CT-133 flew from Ottawa Airport, intercepting the Air Canada jets at top-of-climb.

Fuel from the wing-tanks of each CAAFCER Air Canada flight were sampled and analysed by the DND Quality Engineering Test Establishment (QETE), for hydrogen, aromatics, Sulphur and naphthalene content, and heat of combustion. Fuel samples were taken from biofuel flights prior to dispatch from Montreal Airport, and from JetA1 inbound flights, following shutdown at the arrival gates of Montreal Airport.

Biofuel-blend and Jet A1 contrails were successfully obtained and measured from minima lengths of eight kilometres (forty seconds age) to maxima of approximately ninety kilometres (a contrail age of seven minutes) for 43% HEFA biofuel, and approximately fifty-five kilometres (contrail age of four minutes) for Jet A1. All contrails consisted of heavy condensate in trailing vortices and in the upper jet wake regions, with $_{ICE}$ particle concentrations of several hundred per cubic centimeter. Trailing vortex condensate sublimated with vortex decay.

Each contrail was obtained from a different aircraft, mostly A320 aircraft, but including A321 and a B763 aircraft. The variability of particulate emissions from individual engines and varying engine types is incumbent to the contrail data-set.

Contrail characteristics have been analysed by fuel properties, for which the CAAFCER and ACCESS II contrail data from the CT-133 have been combined. $_{ICE}$ particle number had a strong inverse dependency upon hydrogen content and a mild direct dependency upon sulphur content.

Aggregated power-law parameter identification has been conducted to account for the effects of varying atmospheric conditions (of RH over $_{ICE}$, RH lapse rate and air temperature) upon contrail $_{ICE}$ particle numbers, for each of the fuel types, biofuel-blend and Jet A1. These identifications have been used to adjust contrail $_{ICE}$ particle number, spherical volume and median effective size to the same reference atmospheric conditions, for each fuel type, at which the 43% HEFA-blend reference contrail has lower number, volume and median effective size than that for Jet A1.

1.0 Introduction

The Civil Aviation Alternate Fuels Contrail and Emissions Research project (CAAFCER), addressed the flight research of high altitude contrails formed by jet transport aeroplanes. In particular, the comparison between contrails formed by petroleum jet fuel and biofuel was the principal research topic. In so doing, the project addressed the relationship between the usage of biofuel to reduce soot emissions, in-turn to lower the contrail $_{ICE}$ number.

The CAAFCER project was an award from the Green Aviation Research and Development Network (GARDN) of the Government of Quebec. The research was conducted by a consortium, led by The Waterfall Group, and consisting of Air Canada (AC), SkyNRG, the University of Alberta, Boeing and the NRC. The principal goal of this project was to measure and compare young contrail characteristics from different jet transport fuels, namely petroleum and biofuel blend, over a contrail age of 0.8 to 8 minutes. For such a comparison, the determinant parameters are the types of jet fuel, individual engine, aircraft and atmospheric conditions. The comparative analysis considers the parametric variants of fuel properties (for the JetA1 and 43% HEFA blend used on the experiment) and atmospheric conditions.

The flights were conducted over the period 20th April to the 4th May 2017, for the last biofuel flight, and a subsequent Jet A1 flight on 11th May 2017. Research consisted of the flight measurement of contrails and emissions produced by Jet A1 and by a biofuel blend, consisting of 43% Hydro-processed ester fatty acid (HEFA) biofuel and 57% Jet A1.

Through the process of radiative forcing (RF)-induced heat entrapment, cirrus-transformed persistent contrails increasingly have been viewed as having a significant contribution upon global warming [1]. RF, although complex, can be somewhat related to contrail thickness, described by the $_{ICE}$ particle number density, *e.g.* in overnight heat entrapment. Contrail modeling has connected $_{ICE}$ particle numbers to soot particle emissions [2]. Substantially lower soot emissions from biofuels (at higher hydrogen content than petroleum fuels) have been measured in aero-engine test cell facilities [3]. For HEFA-blends of biofuel, soot emissions are likely to be in the soot-rich range [4], of 10^{14} to 10^{15} particles per/kg, with a theoretical expectation [5] that the number of $_{ICE}$ particles will be dependent upon the soot number, rather than background volatile emitted particles [2].

Contrail measurements made holistically using the NRC CT-133 during NASA project ACCESS II suggested that, for trailing vortex-dominated, non-persistent contrails, $_{ICE}$ particle numbers are reduced for the HEFA-blend compared to petroleum fuel [6, 7]. Project CAAFCER is intended to further research the association between types of jet fuel (whether biofuel or petroleum-based) and contrail development for persistent contrails formed in atmospheric conditions that are dominated by the North American jet-stream, in the area of the eastern seaboard along the St Lawrence Seaway region.

2.0 Experimental details

2.1 Contrail generating aircraft

CAAFCER flights used Air Canada (AC) jet transport aircraft on commercial service flights [13] as the emitting and contrail generating aircraft. In contrail-conducive atmospheric conditions, designated AC flights from Montreal to Toronto flew on the 43% HEFA blend. A fuel sample was taken from wing tanks at dispatch. AC flights from Toronto to Montreal flew on Jet A1. Particular AC aircraft were designated as time-paired for contrail measurement by the NRC research jet, *i.e.* after the 43%HEFA contrail measurement, the NRC jet would hold near Toronto, for the designated AC flight from Toronto to reach top-of-climb, whilst bound for Montreal. Upon arrival at Montreal Airport, a wing tank Jet A1 fuel sample was taken from each designated aircraft. The fuel samples were analysed by the Quality Engineering Test Establishment (QETE) of the Department of National Defence (DND).

2.2 Contrail and emissions measurement aircraft

Contrail and emissions data measurements were made by the NRC CT-133 from Ottawa Airport, intercepting and temporarily flying in-trail at M0.56 behind the 43% HEFA and Jet A1 AC flights, which flew nominally at M0.76.

Thus the CT-133 opened out from the AC aircraft at the nominal rate of approximately 3.7 km per minute. Initial contrail intercept distance was 9.2 km and maximum contrail length measured was approximately 92 km.

The NRC CT-133 contrail and emissions measurement sensors are described in Table 1, and depicted in Figure 1. The FSSP-100, mounted off the starboard pod and used for contrail $_{ICE}$ particle counting and sizing, was carefully calibrated to be sensitive in the smallest bins size of particle, namely a minimum of 0.5 µm. The denuder was upstream of the CPC 3776 and could be valve-switched to either by-pass (CPC3776 would count all ultrafine aerosols) or in-line (denuder temperature controlled to remain >300°C, thereby vapourising all volatile particles).

The Thermo 42I NOx analyser, located in the starboard underwing pod, operated upon the principle of the chemi-luminescence intensity being proportional to concentration for the reaction between NO and ozone. The complete NOx determination required the catalytic conversion of all NO_2 to NO, a relatively long process, so that one reading was available each 20 seconds. Without conversion, a concentration reading was available each second, called streaming mode. In this case, the concentration reading was sensitive to NO and some other nitric compounds such as HONO, but not sensitive to NO_2, which required, firstly, catalyzed reduction to NO for reaction with ozone.

In young aircraft emission plumes and contrails, the majority of nitric oxide compounds is present as NO and oxidises slowly, negligibly over an elapsed time of several minutes. To reflect data

acquisition in the streaming mode without firstly converting the NO_2, the measured parameter was identified as NOy.

Table 1. NRC CT-133 emissions and contrails measurement instrumentation

Sensor location	Sensor	Description	Acquisition rate
Port wing			
Wing surface, outboard	Wing glove, 24 surface pressure sensors	Measures high-rate unsteady aerodynamic forces, for example, during the penetration of trailing vortex cores	600 Hz
Under-wing HAARC pod	LII 300 BC sensor	Measuring BC volumetric concentration, using a forward-facing isokinetic inlet, under control of a mass-flow controller.	20 Hz
Starboard wing			
Under-wing HAARC pod	Isokinetic inlet	Forward-facing particle inlet (for CN and CPC), under control of a mass-flow controller	
	Rear-facing inlet	Gaseous inlet (for NOy)	
	CN 7610 aerosol counter	condensation nuclei counter, >10 nano-metres	10 Hz
	CPC 3776 ultrafine aerosol counter	ultrafine aerosol counter, for particles >2.5 nano-metres in size	10 Hz
	Denuder	non-volatile particle path for CPC 3776 (vaporizes volatile particles) – when bypassed CPC 3776 counts volatile and non-volatile	-
	Thermo 42I	NOx analyser, operated in the streaming mode, hence measuring NOy (majority of young contrail emissions NO, some HONO compounds)	1 Hz
	FSSP-100	Forward-scattering spectrometric probe, measuring particles > 0.5 µm in size – in this environment, $_{ICE}$ particles	20 Hz
Nose	Licor 840A	Atmospheric CO_2 and water vapour mixing ratios	3 Hz
	FIRNS	Inertial reference & navigation system, based upon the HG1700 IMU, Kalman-filter blended with GPS	600 Hz
	Air data boom	Atmospheric pressure and temperature, pitot pressure; incidence and sideslip angles.	600 Hz
	Particle detector probe (PDP)	Measuring $_{ICE}$ particle concentration	20 Hz
Cockpit	Novatel DGPS receiver	GPS	600 Hz
	DAS	Central data acquisition system for all state & sensor parameters	600 Hz
	Line-of-flight video camera	Recording line of flight view (visual spectrum)	60 frames per second

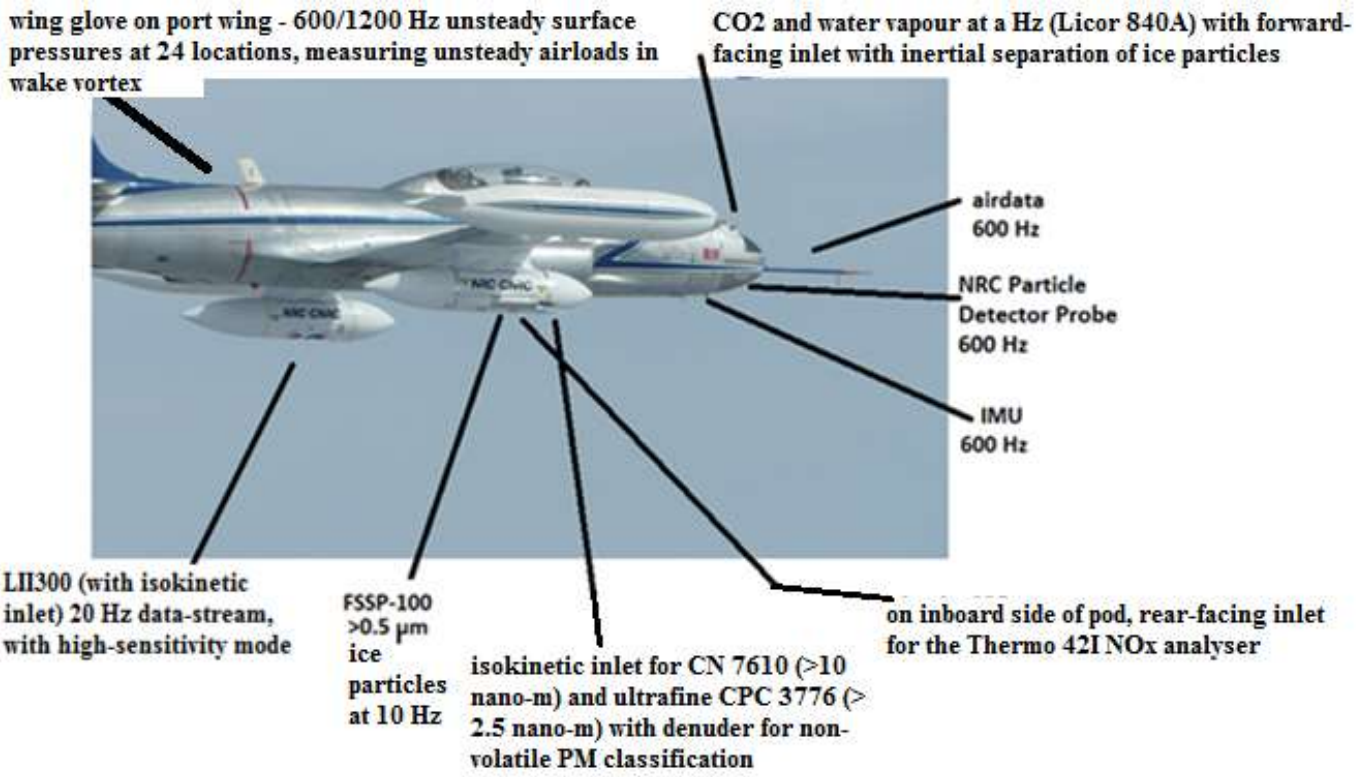

Figure 1. NRC CT-133 research jet, equipped with contrail and emissions measurement sensors for CAAFCER flights.

2.3 Emitter/generator engine operating condition

As earlier described, CAAFCER contrail-generating flights consisted of Air Canada commercial service flights between Montreal and Toronto [13]. Contrail and emissions data was obtained, using the NRC CT-133 flying in-trail.

The Air Canada flights were flown under an economically-optimised, designated Cost-Index (CI) on the aircraft FMS. The CI optimized engine thrust levels for flight sector length and winds, so as to blend minimum fuel consumption and minimum time delay. This auto-flight management resulted in cruise speeds of M 0.74 to 0.76 (varied with cruise altitude and aircraft weight). This Mach Number range was design-representative for the A320 aircraft type.

For the majority of the CAAFCER flights, specific flight data was recorded inflight on a PCMCIA card in the Quick-Access Recorder (QAR). The card was removed at the gate, upon arrival. By this process, engine operating points were available for most of the flights, insofar as card-recording was not successfully retrieved for some flights.

Engine operating points varied little between flights, as observed in the summary table below. With reference to this table, typical de-rated Take-off/Climb thrust settings are: N_1 91%, TGT

760°C, total fuel-burn 7.5 metric tonne per hour (mt/hr). Cruise operating points were in the range N_1 80-86%, TGT 570-600°C, and fuel-burn 2.4-2.7 mt/hr, combined. These conditions represented a ±3% variation around the mean values, which is a relatively small difference range between aircraft, from a contrail and emissions viewpoint. Nevertheless, some variation of particulate matter emissions between individual engines could be expected.

Table 2. List and details of Air Canada (AC) flights used on CAAFCER contrail research flights.

Date	Flight Aircraft and Engine types	Fuel	Cruise conditions (during CT-133 contrail measurement)						
			Flight level	M	Total fuel burn (mt/hr)	Left engine		Right engine	
						N_1	TGT	N_1	TGT
20Apr17	ACA407 (A320) CFM56-5A1	JetA1	FL320	0.76	-	-	-	-	-
25Apr17	ACA401 (A320) CFM56-5A1	43% HEFA	FL340	0.754	2.50	85.8	602	85.8	603
28Apr17	ACA454 (A321) CFM56-5B3-P	43% HEFA	FL320	0.765	2.56	82.8	588	82.8	588
	ACA457 (A321) CFM56-5B3-P	JetA1	FL330	0.757	2.70	84.6	614	84.4	613
03May17	ACA415 (A320) CFM56-5A1	43% HEFA	FL340	0.76	-	-	-	-	-
	ACA412 (B763) CF6-80C2 B1F/B6F	JetA1	-	-	-	-	-	-	-
04May17	ACA239 (A320) CFM56-5A1	JetA1	FL310	0.736	2.50	80.9	572	80.9	573
04May17	ACA241 (A320) CFM56-5A1	43% HEFA	FL320	0.764	2.57	82.4	582	82.4	595
	ACA235 (A320) CFM56-5A1	JetA1	FL310	0.741	2.39	80.2	562	80.2	558
11May17	(A320) CFM56-5A1	JetA1			-	-	-	-	-

2.4 Aircraft type and engine variability

Each of the CAAFCER flight contrails emanated from a different aircraft tail number, and therefore emanated from different engine serial numbers. Aircraft type was generally A320, but two A321 and a single B763 were other aircraft types used on CAAFCER Air Canada flights. Thus, the analysis that can be conducted is based upon the premise of exploring fuel property effects and atmospheric effects upon contrail characteristics, for the range of differing engine types and serial numbers.

3.0 Results and discussion, general

3.1 Contrail type

All CAAFCER contrails (from A320, A321 and one B763 aircraft) were Upper Jet Wake (UJW) type, mostly UJW-stem with some extent of UJW-lateral crown. All had limited Trailing Wake Vortex (TWV) condensate. The contrails were generally non-homogenous vertically and asymmetric laterally. Rather, their cross-sections tended to be lumpy or puffy, and wavy laterally. Crosswind shear effects were evident, in the UJW stems being slanted laterally. The contrails on the 28th April were visibly sublimating; all other contrails were lasting over the period of measurements.

In comparison, ACCESS II contrails, generated by the singular NASA DC-8 at M 0.8, were sublimating TWV-type, dominated by Wake Vortex (WV) dynamics and with very little UJW condensate present.

Inflight photographs (line-of-flight, LOF, video stills) of contrail states are shown in Figure 2.

3.2 Atmospheric conditions

CAAFCER flights were conducted in the Upper Troposphere Lower Stratosphere (UTLS) atmosphere of the St Lawrence Seaway, between Toronto and Montreal, under jet-stream influence. Atmospheric characteristics included frequently-occurring, localized patches of falling and sublimating cirrus $_{ICE}$ particles (sometimes described as ‘mare’s tails’), which are evidence of high $_{ICE}$ particle growth rates. Spatially non-homogenous atmospheric states, of varying spatial scales, typically 10-100 km, were encountered by the CT-133 on CAAFCER flights.

Generally, westbound (43% HEFA blend with JetA1, conducted in Montreal) flights flew higher, in colder air temperatures and higher Relative Humidity (RH) conditions (more conducive to thickened contrail formation), with greater time in-cruise, because of headwinds. On the other hand, eastbound (baseline JetA1) flights had less time in cruise and flew at lower altitudes, generally slightly less conducive to contrails. In addition, aerodrome works at Toronto caused greater delays, so that eastbound flights tended to have greater time imperative (*i.e.*, to make-up time delays), inducing lower-cruise altitudes also.

Overall, the amount of Jet A1 contrail data was approximately half that of 43% HEFA-blend contrail data. Totals of sixteen 43% HEFA-blend and ten JetA1 re-constructed contrail cross-sections were accumulated through the course of CAAFCER flights and data analysis.

Figure 2 – CAAFCER inflight pictures of contrail states, *top*, slanted-veil state of UJW contrail stem, and *bottom*, laterally-spreading UJW contrail crown of cirrocumulus character.

4.0 Analysis

4.1 Overview of contrail and emissions data analysis methodology

Contrail and emissions cruise flight data for biofuel and petroleum jet fuel, has been analysed in the spatiotemporal domain, for which the primary spatial variables of dynamic change were in the lateral and vertical directions, orthogonal to the contrail axis. Contrail and emissions plume cross-sections were re-constructed from concatenated sub-sets of nine passes across the contrail (occupying an elapsed time of, typically, two minutes). An example of flight-path concatenation, used to reconstruct a single contrail cross-section, from nine flight-path segments across the contrail, is shown in Figure 3 and discussed further in the next section.

By this methodology, spatially-referenced re-constructions of GARDN CAAFCER contrail cross-sections have been conducted for four biofuel (43% HEFA/JetA1) contrails and six baseline JetA1 contrails, using a total of ten different jet transport aircraft, of three types (A320, A321 and a B763). Analysis therefore can be based under the premise of considering contrail characteristics variations and potential parameterisations with fuel properties and atmospheric properties, across the range of individual engines, engine types and aircraft types.

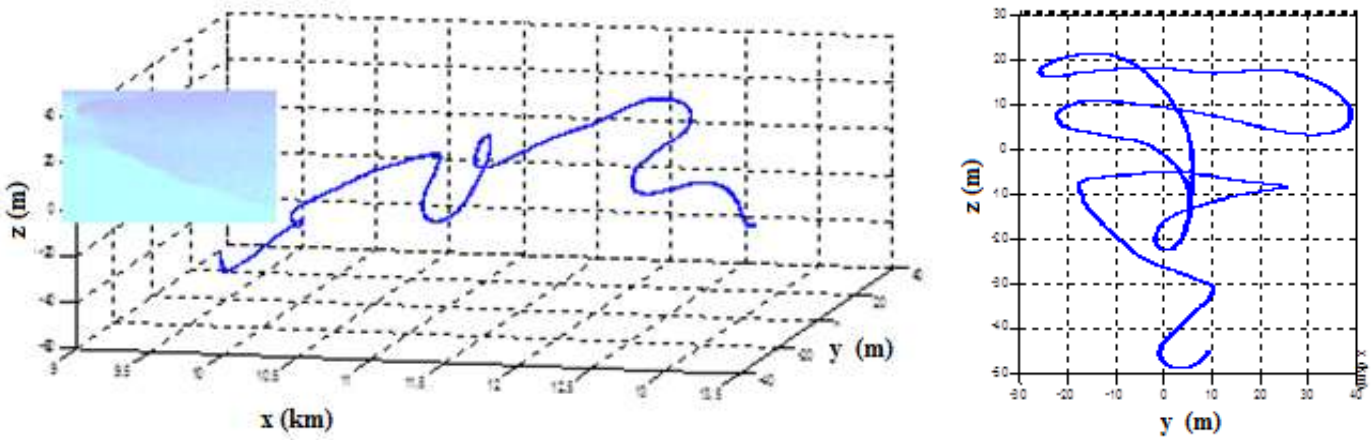

Figure 3, A recorded flight-path segment from the NRC CT-133 during a contrail measurement survey: (left), isometric view, predominantly shown along the contrail (x-axis), (right) end-view, showing the nine flight-path segments across the contrail, from which are re-constructed a single, autonomous cross-section of the contrail.

Using NRC Gas Turbine Laboratory (GTL) test cell nvPM emissions data on the effects of total hydrogen [3] and NASA/Aerodyne flight data on the effects of sulphur on PM [5], the Forward-Scattering Spectrometric Probe (FSSP) Apparent Emission Index by $_{ICE}$ particle number (AEIn) contrail data was compared and parameterised by fuel properties for each flight. Observed trends in the data enabled adjustment of contrail $_{ICE}$ particle count, to mean values of hydrogen and sulphur content, as reference values.

Thereafter, the 'fuel-adjusted' contrail data has been log-normal parameterised for variations in atmospheric conditions, for the length of each contrail.

This analytical procedure has enabled comparison of JetA1 and biofuel-blend (43% HEFA/JetA1) contrails, amidst variations of fuel properties and atmospheric conditions.

4.2 Re-constructed contrail cross-sections

The high-rate, high-fidelity inertial and airdata recorded by the NRC CT-133 is used to re-construct contrail and emissions plume cross-sections [3,4]. For this purpose, lateral and vertical flight traverses of the contrail were spatially re-assembled, concatenated and interpolated to provide contours of $_{ICE}$ particle number density, or emitted species number density for solids or volumetric concentration for gases. The contour plots were integrated. The integrands were then divided by the fuel burn per metre air distance, to derive $_{ICE}$ particle number AEIn (or other state-parameter of emission species EI, by number or mass).

Typically nine traverses were used for each cross-sectional re-construction, but upon *a priori* experience, as few as five traverses might be used, if they provided sufficient plume cross-sectional coverage, for veracious, interpolative contouring of species concentrations.

Typically 2-3 minutes of flight-time traverses are required for one plume re-construction, occupying 10-16 nautical miles of down-track airspace, and during which time emission plume/contrail length typically increased by 3-6 nautical miles. The re-constructed contrail cross-sections are an average, also, of the atmospheric background conditions over each measurement segment of the contrail. The background atmospheric parameters of influence (upon contrail development) are air temperature, RH over $_{ICE}$ (RH_{ICE}) and RH lapse rate, $\partial RH/\partial z$. These parameters were found by measurement to typically change along track in a variety of spatial scales, with resultant patches of $_{ICE}$ particle growth or sublimation – all reflected in AEIn values for each re-constructed contrail cross-section.

Spatial re-construction is an averaging process. As such, this reduces the inaccuracy effects of uncertainties such as contrail lateral meandering) and vertical reference (whether geo-centric or wake vortex referenced). Nevertheless, the uncertainties determine the process to be probabilistic. Examples of re-constructed contrail cross-sections are shown in Figure 4.

Note, in Figure 4, the lateral and vertical scales are different. A320/321 generated contrails tended to be 150-200 metres in depth and within $\pm$30 metres in width, *i.e.* contrail aspect ratios, total width / height, in the range 0.3-0.4. The B763 contrail was of similar depth, approximately 150 metres, but of greater width, namely $\pm$80 metres. This was probably associated with the greater lateral separation of the trailing vortices – the present data quantified the A320/321 vortex lateral separation as 50-60% wingspan, less than that of B763 aircraft70-80% wingspan. For this probable reason, the vortex-induced downdraught and pressure expansion was greater for A320/321 aircraft, and hence lateral containment of emissions and contrail.

On A320 contrails of longer length (>37 km), with developing UJW crown structures, lateral spreading was measured beyond this extent.

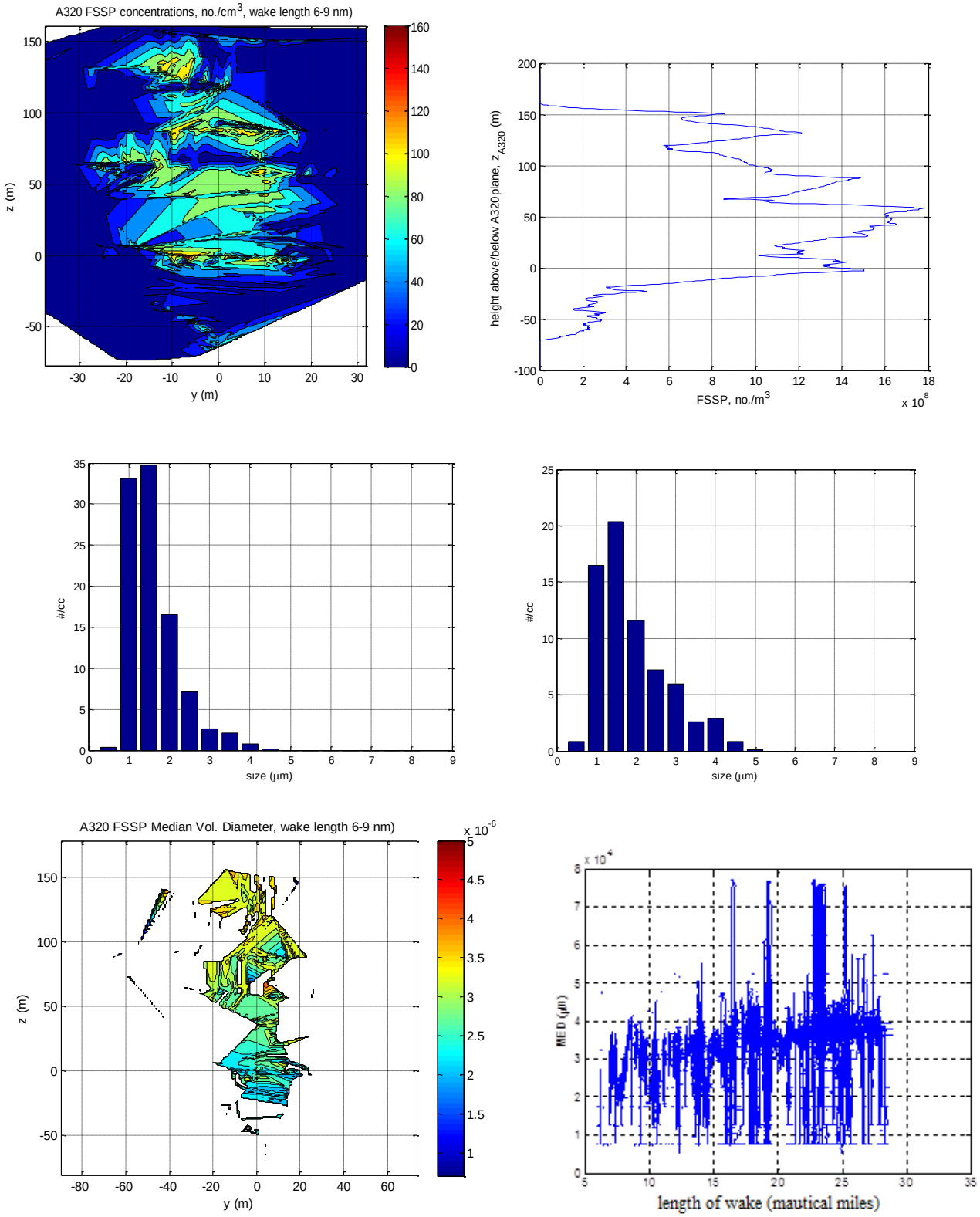

Figure 4 – *top, left,* typical contrail cross-section, and *right,* vertical distribution of $_{ICE}$ particles; *mid, left to right,* $_{ICE}$ particle size spectra, *bottom, left,* MED contrail cross-section, *right,* trend of MED with contrail length.

4.3 Contrail emission index summary, $_{ICE}$ particles & aerosols

CAAFCER contrail FSSP AEIn, together with EIn for Condensation Nuclei (CN $\geq$ 10 nano-m), ultra-fine aerosols from the Condensation particle Counter (CPC, $\geq$ 2.5 nano-m) and non-volatile CPCnv (*i.e.*, denuder in-line operation), are presented in Figure 5. The low FSSP AEIn delineation in the sublimating JetA1 and 43% HEFA contrails of the 28th April are evident. For these, the CN and CPC EIn values were substantially lower, by an order of magnitude, than values in the other, lasting contrails.

As seen from Figure 5, in differing atmospheric conditions (for the operational reasons explained above), the 43% HEFA/JetA1 contrails measured greater $_{ICE}$ particle number density than the JetA1 contrails, which occurred at lower cruise altitude, with slightly lower RH_{ICE}, higher atmospheric temperature (T_S) and lower (positive) RH lapse rate (meaning the 43% HEFA-blend contrails could be expected to have a greater propensity for $_{ICE}$ particle growth in the UJW crowns).

Thus, these differences are required to be accounted for in the atmospheric parameterisation model. Mean atmospheric parametric values, for the measured contrails, are shown in Table 3. For the analysis of contrails, the locally measured and derived T_S, RH_{ICE} and $\partial RH/\partial z$ were applied to each re-constructed contrail cross-section parameterization.

Table 3. List and details of Air Canada flights used on CAAFCER contrail research flights.

Fuel	Atmospheric parameter mean values		
	T_S (°C)	$\partial RH/\partial z$ ($\%m^{-1}$)	RH_{ICEce} (%)
JetA1 (A320/B763)	-44	0.013	97
43% HEFA/JetA1	-48	0.045	103

As a percentage, CPC nvPM EIn values were 2-10% of CPC PM EIn. CPC PM (*i.e.* volatile and non-volatile) EIn values were typically 200-500% of CN EIn, implying the 100-400% of particles being sized between 2.5 and 10 nano-metres, essentially all being volatile. Although there is no sizing information available other than this, the figures imply [volatile / nv] ratios between 20 and 250, in agreement with [5], a ratio of 120 for 0.068% Sulphur. Nevertheless, shattering of particles at the isokinetic probe inlet cannot be discounted, either. For B763, A320 and A321 JetA1 contrails, FSSP and CN, CPC values were of similar magnitudes, between differing aircraft Types.

As implied by the CPCnv and FSSP-100 AEIn Figure 5, the highest inferred values of activation ($_{ICE}$ deposition on soot particles), represented by the measured ratio [FSSP AEIn] / [CPCnv EIn],

were of the order of 10%. Figure 6 compares CAAFCER contrail data with that of other contrails (from a variety of aircraft and engines, and obtained in a variety of atmospheric conditions) measured by the NRC CT-133, plotted against CN EIn (only, i.e. the CPC data is not included). The approximate trend of greater aerosol content and greater contrail $_{ICE}$ particle number is observed in this figure. In particular, the CAAFCER contrails were of the highest AEIn, *c.f.* any previous measured by the NRC CT-133, and on-average an order of magnitude higher than ACCESS II contrails.

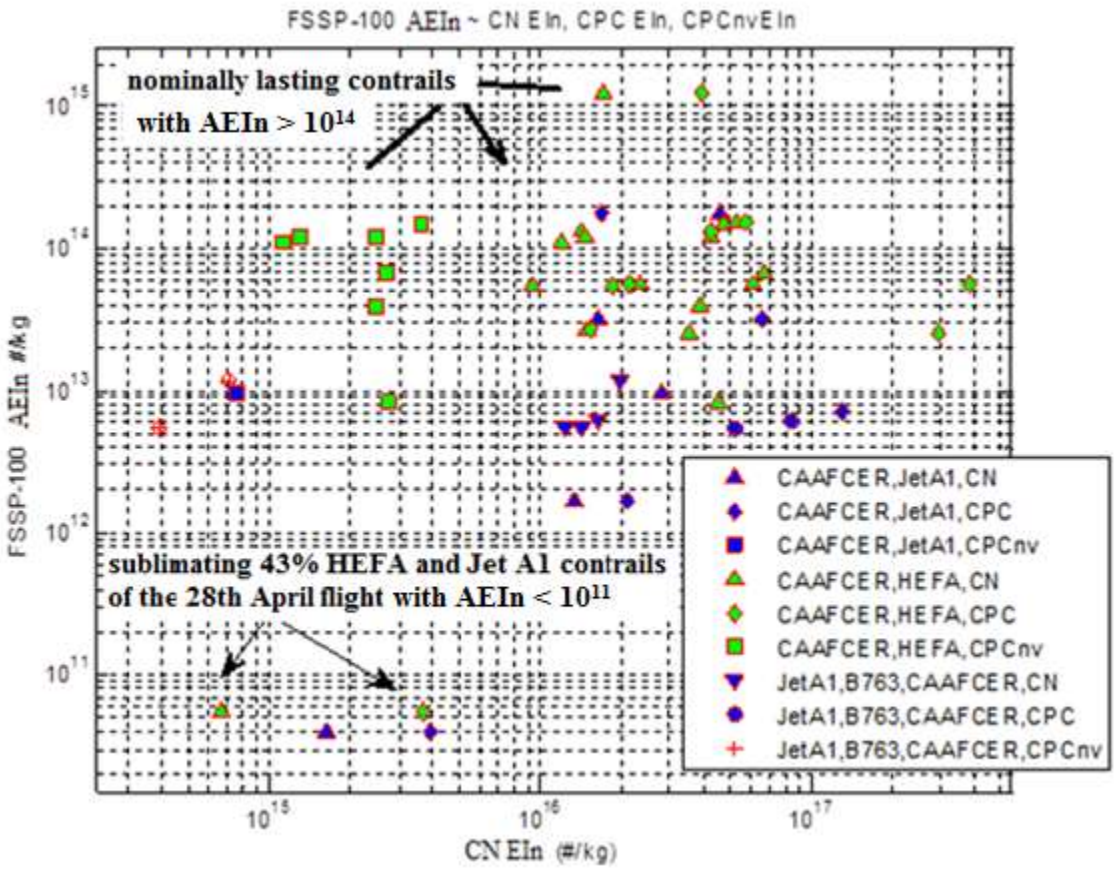

Figure 5 – plot of CAAFCER contrail AEIn values, for the FSSP-100 against CN, CPC & CPCnv values, as an assemblage of NRC contrail data from a number of projects, 2012-2017 (*note*, pointers at the top part of the graph indicate those AEIn values obtained from lasting contrails, AEIn >10^{14} for these generators; pointers at the bottom part of the figure refer to sublimating, faintly-visible or invisible contrails, AEIn < 10^{11} per kg).

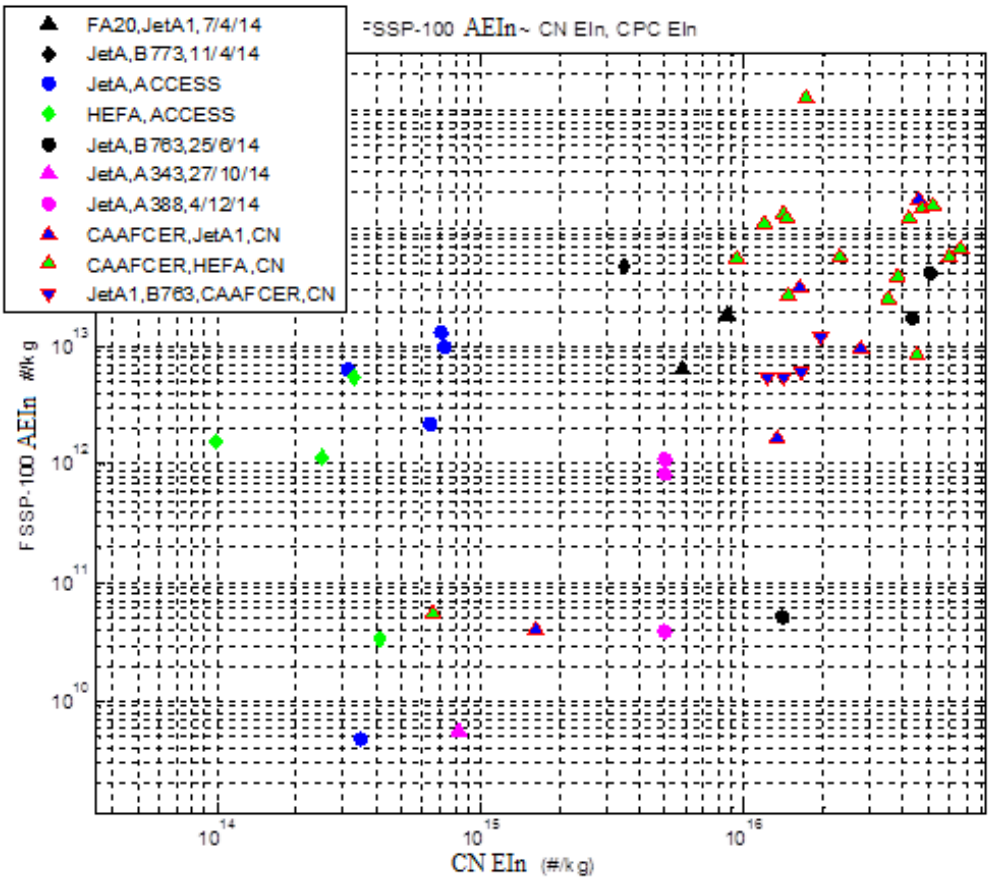

Figure 6 – plot of all contrail AEIn values, derived from contrail cross-sections, measured by the NRC CT-133, and compared to CN EIn [7].

5.0 Contrail AEIn parameterisation with fuel properties

5.1 Fuel properties

QETE undertook testing of wing-tank fuel samples for both Jet A1 and 43% HEFA-blend, to analyse for: (1) heat of combustion, (2) total hydrogen, (3) sulphur content, (4) naphthalene content, and (5) aromatics content. In addition, Intertek undertook aromatics content testing of the all samples.

Results [8] showed significant variations in properties, e.g. sulphur content between 0.03 % and 0.11 %. Mean values of sulphur content were 0.058% for JetA1 samples and 0.052% for 43% HEFA/JetA1 blend. The first wing-tank 43% HEFA-blend fuel sample yielded the highest, apparent sulphur content value of 0.11%. This value was confirmed by re-testing and was therefore likely to actually be principally undrainable Jet A1 from the sump region, as discussed below.

Total hydrogen content, by test, varied between 13.6% and 13.8% for Jet A1, and 13.7% and 14.1% for 43% HEFA/JetA1; mean values were 13.74% for JetA1 and 13.92% for HEFA-blend.

Thus, although mean values of sulphur and hydrogen content trended in the correct sense between JetA1 and 43% HEFA-blend (hydrogen content increasing and sulphur content reducing), the properties of individual HEFA-blend fuel samples varied substantially between individual aircraft, for the same nominal fuel, whether 43% HEFA/JetA1 or JetA1 (albeit, JetA1 from different regions and hence refinery sources across the continent). For the 43% HEFA/JetA1, the differences could be probably explained by fuel tank sump residual contamination, following the incomplete de-fuelling prior to refuelling with 43% HEFA-blend. Residual sump fuel would consist of inbound Jet A or Jet A1 with an expected sulphur content within the Jet A or Jet A1 specification range. The highest sulphur content of 0.11% was taken from an A320 inbound from Calgary in western Canada. Sulphur limits by Jet A1 specification CAN/CGSB3.23-2016 were 0.3% by mass.

Thus, in order to improve the estimation of critical test fuel properties, relating to contrail formation, the following methods have been used

- Tanker analyses of fuel properties [8] (in particular, sulphur content, fuel density, distillation curves) have been examined for the following fuels, for consistency
    - Pure HEFA batch, delivered by Alt Air (i.e., 100% HEFA, simply factored down to 43%)
    - JetA1 batch analysis from the supplying refinery, used for HEFA blending; and
    - Final, bowser 43% HEFA-blend
- In particular, the 43% HEFA-blend analysis [13] is subsequently used, for the properties of the HEFA-blend uploaded into the A320/321 fuel tanks with the following considerations
    - This analysis did not include the measurement of total hydrogen content (THC); rather, ASTM D3343-16 has been as programmed by QETE [12]. This is a method of THC estimation based upon the inputs of aromatic content, distillation curve and fuel density. When compared to the NMR measurement of THC [8], the method accurately estimated THC (tending to under-estimate by 0.1%) in all but 1 of the 10 fuel sample cases;
    - Applied to the 43%-HEFA blend fuel analysis values, ASTM D3343-16 (with an increment of +0.1% for the afore-mentioned under-estimation of content) resulted in a THC of 14.56
        - Finally, this THC is adjusted for 300 kg of residual JetA1 in the A320/321 fuel tanks (following defueling), when the aircraft is refueled with 43% HEFA-blend; final THC values for the five flights were 14.56 ± 0.005;
        - Sulphur content of the 43% HEFA-blend was treated similarly for the residual Jet A1 fuel, to arrive at a content of 0.052%.

The Jet A1 properties for the petroleum jet fuel contrail cases were in accordance with the analysed wing-tank fuel samples taken from the arriving aircraft, all of which may have contained

JetA1 from more than one aerodrome source. A summary of measured (for Jet A1) and derived fuel properties (for 43% HEFA blend) is shown in Table 4.

Table 4. List of fuel properties for Air Canada CAAFCER flights, Jet A1 from arriving aircraft fuel samples, 43% HEFA-blend from bowser fuel analysis, adjusted for residual tank Jet A1.

Flight	25th April 2017		28th April 2017		3rd May 2017		4th May 2017 (1)		4th May 2017 (2)	
Property (% mass)	JetA1	43% HEFA	JetA1	43% HEFA	JetA1	43% HEFA	JetA1	43% HEFA	JetA1	43% HEFA
Sulphur	0.07	0.052	0.08	0.052	0.04	0.052	0.07	0.052	0.03	0.052
Hydrogen	13.8	14.56	13.6	14.56	13.8	14.56	13.7	14.56	13.8	14.56

5.2 Hydrogen content effect upon emission and contrail particles

Figure 7 displays engine test cell data [3], demonstrating an asymptotic reduction of BC mass emissions with total hydrogen content, percentage by mass. Reference 1 EIm data, obtained from test cell operations on a Microturbo TRS-18 turbojet engine, provided very good correlation against total hydrogen content, and better correlation, than against either aromatics content or smoke point.

Using this relationship for non-volatile particulate mass emissions as guidance, the contrail EIn data for CAAFCER and earlier NRC data from NASA ACCESS II, has been similarly investigated. Figure 6 plots contrail FSSP-100 AEIn against hydrogen.

Whereas CAAFCER data include a number of different aircraft flying at differing altitudes at constant power $\pm$3%, the ACCESS II data was all obtained from the same engines (those of the NASA DC-8) under similar atmospheric conditions for the different fuels, the Jet A and 50% HEFA/JetA blend, at a constant power setting of normal-rated thrust (M0.8). Furthermore, the two ACCESS II fuels had similar sulphur content, by a custom NASA specification, *i.e.* the JetA was very low sulphur, 0.00085% mass (compared to the 0.052% and 0.03-0.07% sulphur, respectively, for the 43% HEFA-blend and the JetA1 fuels of CAAFCER).

Hence, total hydrogen content (THC) was the principal parametric variation in the Figure 7 plot of the NRC data from NASA ACCESS II contrails. It is seen that, in spite of being different aircraft and engine types to CAAFCER data, the ACCESS II Jet A contrail data quantified similarly to CAAFCER Jet A1 data points, whereas the majority of CAAFCER 43% HEFA data clustered more consistently (a reflection on consistency of atmospheric conditions for the majority of data points), in exceedance of ACCESS II 50% HEFA data. For all data, there are large variations of AEIn values due to atmospheric state variations, aircraft and individual engine variations and potentially variations in other fuel properties.

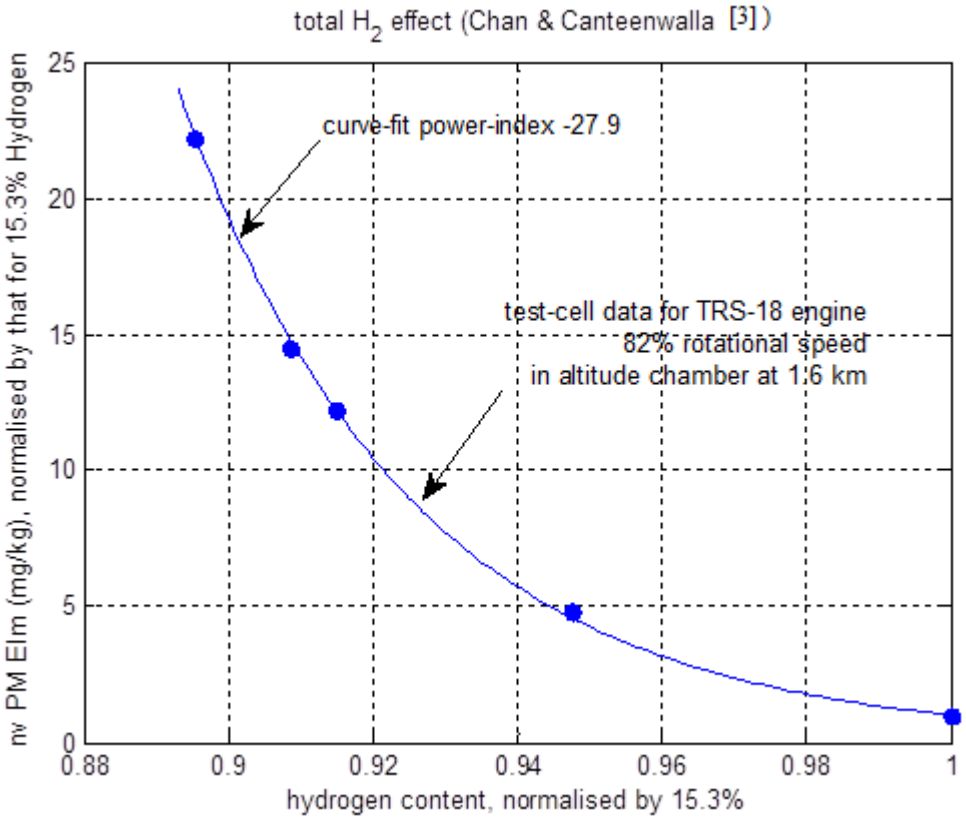

Figure 7 – plot of nvPM EIm against total hydrogen content (normalised by 15.3%) for five jet fuels tested in the altitude chamber of the Gas Turbine Lab of the NRC1; curve-fit is the variation nvPM EIm ~ (total hydrogen)-27.9.

If ACCESS II Jet A, CAAFCER Jet A1 and ACCESS II 50% HEFA-blend data points are included in a log-log curve fit for the identification of the total hydrogen effect (Figure 8), the power-index of the fit is -36. As noted in Figure 8, the variations of AEIn (ordinate axis) were broad and attributable to variations in background atmospheric conditions, between sub- and super-saturation, air temperature biases (43%HEFA-blend flights had biases of colder air temperature higher RH_{ICE} magnitudes, and were not included in the fit). Thus, this identification is principally influenced by the ACCESS II Jet A and 50% HEFA contrail data, which were generated by the same aircraft, engines and in similar atmospheric conditions (all contrails visibly sublimated at ages of 1.5 to 3 minutes) for the two fuel types.

The contrail $_{ICE}$ particle AEIn (mean value thereof, for a variety of atmospheric conditions, at any particular hydrogen content percentage) reduced with increasing hydrogen content, at an approximately similar rate to the BC EIm of the test cell data [3], power indices of -36 and -28, respectively. A power-index of -28 has been used for normalising the contrail $_{ICE}$ particle number to a reference hydrogen content, in this case a reference value of 13.74%.

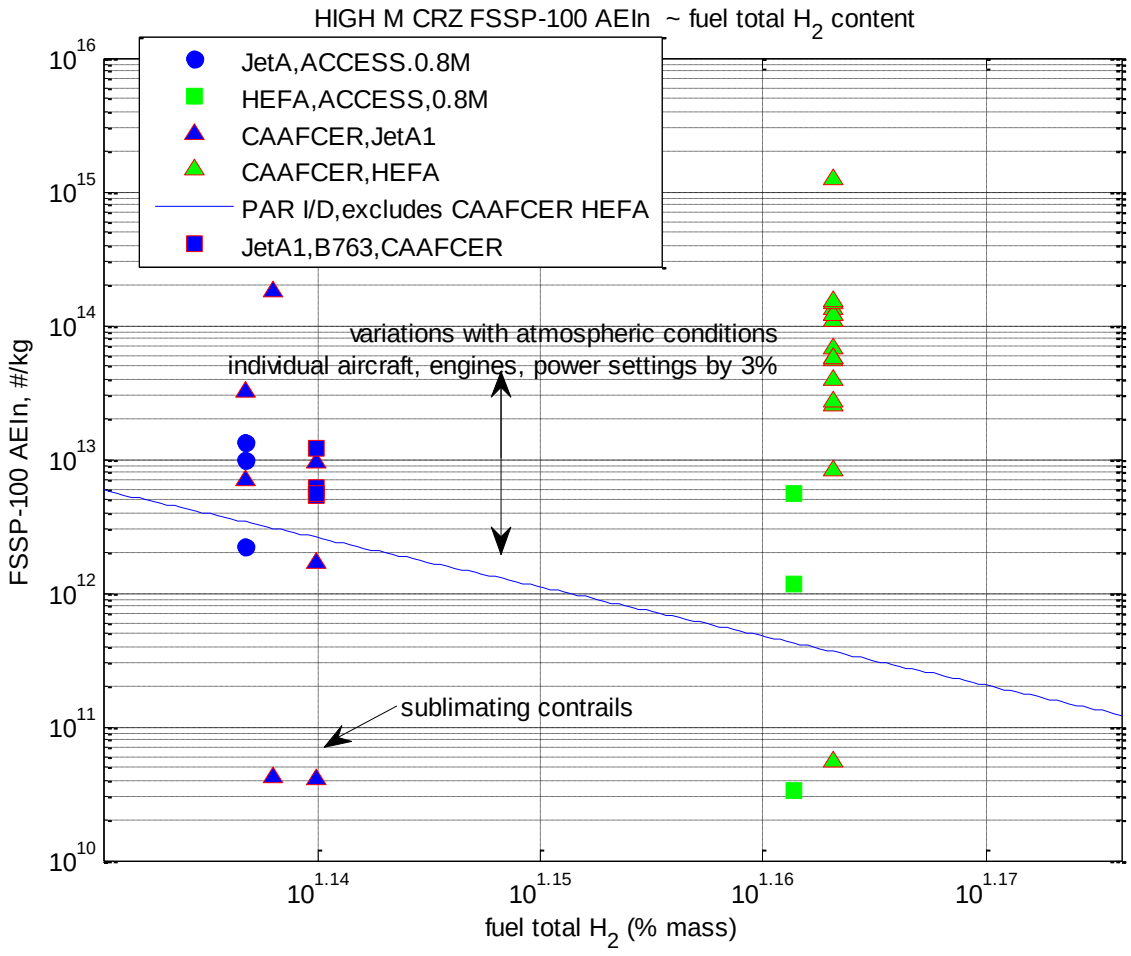

Figure 8 – plot of contrail FSSP-100 AEIn against total hydrogen content; ordinate direction spread includes the effect of variations in atmospheric conditions, such as RH_{ICEICE}, individual aircraft, engines, power settings±3%; the log-log linearization shown is for CAAFCER JetA1 and ACCESS II Jet A and HEFA-blend., resulting in a power index of -36.

5.3 Sulphur content effect upon emission and contrail particles

NASA and Aerodyne conducted flight experiments on the effects of sulphur (S) content on particulate emissions [5]. Figure 1 of [5] provided some guidance on quantifying the effect of S on PM EIn, from which is drawn the approximate, normalised data of Figure 9. An exponential direct relation from the origin is observed in the figure, between normalised S and EIn. Curve-fit to this data of [5] resulted in an S content exponent of approximately 2 for particle emissions EIn, *i.e.* $EIn \propto S^2$.

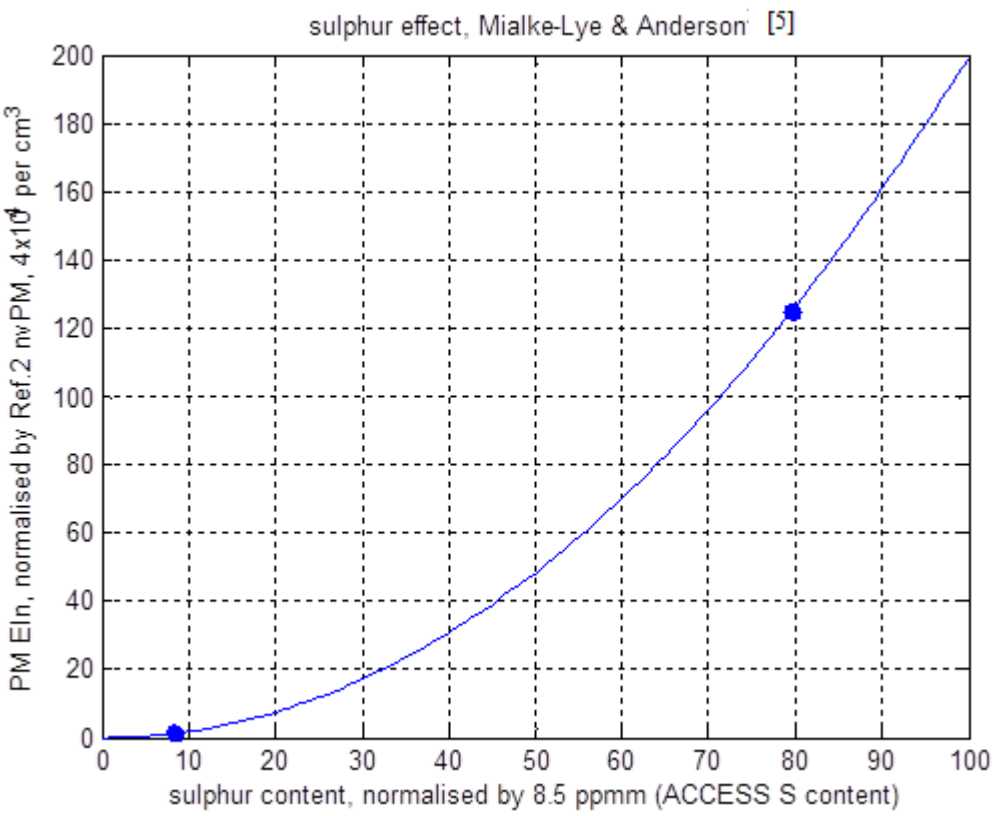

Figure 9 – plot of normalised emitted PM EIn against sulphur content, estimated from Aerodyne/NASA data [5].

To assess the comparison between this PM EIn effect of Sulphur [5] and that of contrail FSSP AEIn, the CAAFCER data (and ACCESS II data, for which the engine operating point. Maximum continuous thrust (MCT), was comparable; atmospheric conditions were sub-saturation and contrails were sublimating at ages of 1.5 to 2 minutes) was firstly adjusted for variations of total hydrogen. This was accomplished in accordance with the results of the previous section, using a power-index of -28, correcting to the CAAFCER mean hydrogen content value of 13.74%.

Subsequently, the hydrogen-normalised contrail FSSP AEIn data has been plotted against the measured sulphur content in Figure 10. It is seen that the plot appears to show a mild correlation between FSSP AEIn and sulphur content, significantly less than the PM EIn correlation of the Aerodyne/NASA data [5] of Figure 9, for which the data suggests a PM EIn exponent of 2, for variation with S. If all CAAFCER and ACCESS II (M0.8) contrails are included in the S correlation, the approximate power index correlation was FSSP AEIn $\propto S^{0.55}$.

For subsequent atmospheric correlation, a contrail FSSP AEIn exponent of 0.55 (*i.e.* FSSP AEIn being proportional to $S^{0.55}$) has been applied to adjust the contrails to the normalised S content

value of 0.0574%, which was the mean CAAFCER value from wing-tank fuel samples (2 x 5 aircraft).

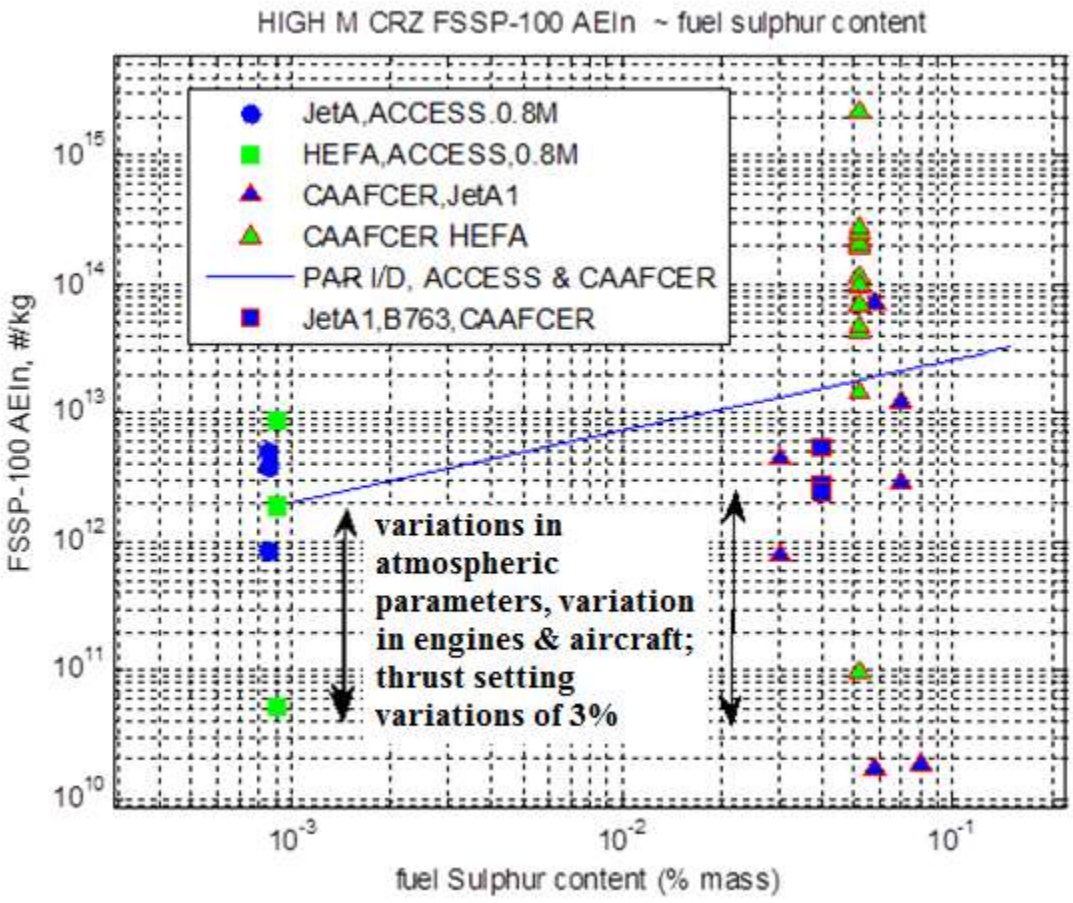

Figure 10 – plot of CAAFCER & ACCESS II NRC data of FSSP-100 AEIn against sulphur content, having first adjusted each contrail AEIn for variations in fuel hydrogen content.

6.0 Contrail AEIn parameterisation, atmospheric properties

6.1 Atmospheric properties

As used earlier, in the reduction of NRC contrail data [4] from NASA ACCESS II, consequential atmospheric parameters for the formation of cruising flight contrails included atmospheric temperature, relative humidity over $_{ICE}$ (RH_{ICE}), and relative humidity lapse rate ($\partial RH/\partial z$). The last parameter was observed [7] to be consequential for contrail AEIn, for the TWV contrails of the DC-8 in the background atmosphere (given that the trailing vortices, and hence contrail, was descending). Nevertheless, RH lapse rate has been retained as an influential parameter for CAAFCER contrails due to the observations and measurements of the contrails having been laterally spreading at the UJW crown, when RH was greatest at the UJW crown level (implying positive lapse rate).

These parameters were lumped [7] into a product-power-law, for which individual parameter relationship guidance was only used for the effect of RH_{ICE} – in particular, the power-law proportionality of $_{ICE}$ particles $\propto RH_{ICE}^{2/3}$ from [9], was used.

In order to improve atmospheric correlation, a different approach has been applied to CAAFCER contrail data, a three-fold approach as follows:

- Log, rather than linear, product-power-law was applied, *i.e.*, $AT_S^a RH_{ICE}^b (\partial RH/\partial z)^c = \log_{10}[\text{FSSP AEIn}]$;
- Individual atmospheric parametric functional relationships were sought, using the criterion of *enveloping* FSSP AEIn values, when cross-plotted against individual atmospheric parameters; and
- The effects were normalised for each atmospheric parameter, considered individually, in order that the weighting of each parameter was correctly identified; in this form log10[FSSP AEIn]/a = 1 at the mean value of the lumped-lower-law parameter for the test data.

In considering the effect-functionality of the individual atmospheric parameters, the JetA1 and 43% HEFA/JetA1 contrails were initially lumped together. Thereafter, maximum-likelihood-estimate functional identifications were conducted for both lumped contrail data-set and for individual-fuel contrail data-sets.

Concerning differing aircraft types and engine serial numbers, B763 and A320/321 contrails were considered together – both were of a UJW stem/crown character, and as shown below had similar FSSP AEIn values for similar atmospheric parametric values.

In the following plots, AEIn was multivariate. Thus, in sequential plots against a single atmospheric parameter, variations in AEIn due to variations in other atmospheric parameters were inherent. For this principal reason, enveloping functional relationships were sought (rather than fitted-data lines) by qualitative inspection of the data-plots.

6.2 Atmospheric temperature

When contrail FSSP AEIn data-points were adjusted to reference H and S content (*per* the Section 5 methodologies) and plotted against atmospheric temperature (Figure 11), a rise-and-fall in FSSP AEIn with reducing atmospheric temperature is observed.

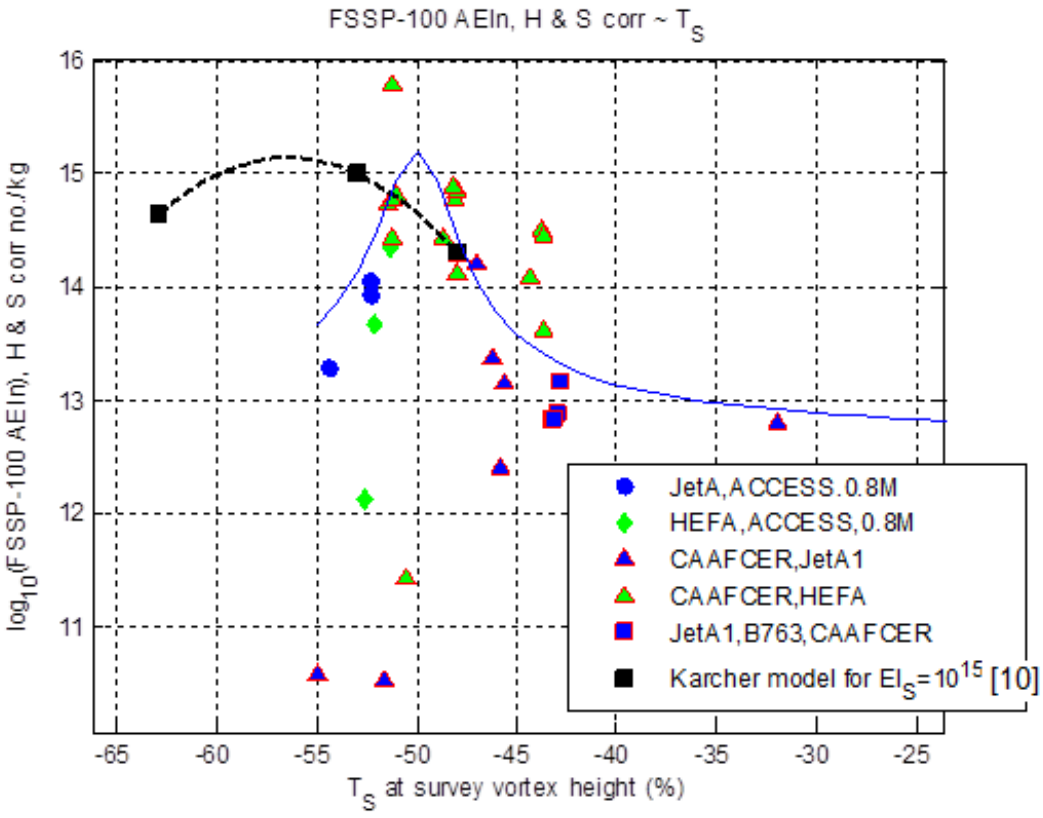

Figure 11 – plot of CAAFCER & ACCESS II NRC data of FSSP-100 AEIn against atmospheric temperature.

A rise with reducing air temperature from -40°C to -53°C has been predicted in modeling [10], from which the AEIn values for $EI_S=10^{15}$ are shown in Figure 11. Although very low temperature contrail data has not been captured in NRC data from ACCESS II and CAAFCER, perhaps a reduction in FSSP AEIn with very low air temperature could eventually be expected due to the inevitably associated reduction in water vapour mixing ratio. Thus, including this deduction, the observations and expectation suggest a 'damped-resonance' type of function. Due to the limited T_S range of the data, the uncertainty in T_S for curve-peak would be unlikely to be consequential in fitting such a type of functional relationship to the flight data. The chosen functional relationship type of curve is shown in Figure 11.

6.3 Atmospheric relative humidity over $_{ICE}$, RH_{ICEce}

Concerning the effect of atmospheric RH_{ICE} upon contrail FSSP AEIn, the NRC data [6,7] from ACCESS II was treated as ~ $RH_{ICE}^{2/3}$, in accordance with the flight data treatment of [9]. For CAAFCER data, an error-function (*erf*) relationship has been applied, as shown in Figure 12. Perhaps *erf* is more reflective of the nature of phase change physical processes, which is a process of deposition of water vapour as $_{ICE}$ on nucleating particles. As observed in Figure 12, an *erf* curve-fit has been aptly centred upon an RH_{ICEce} value of 85%.

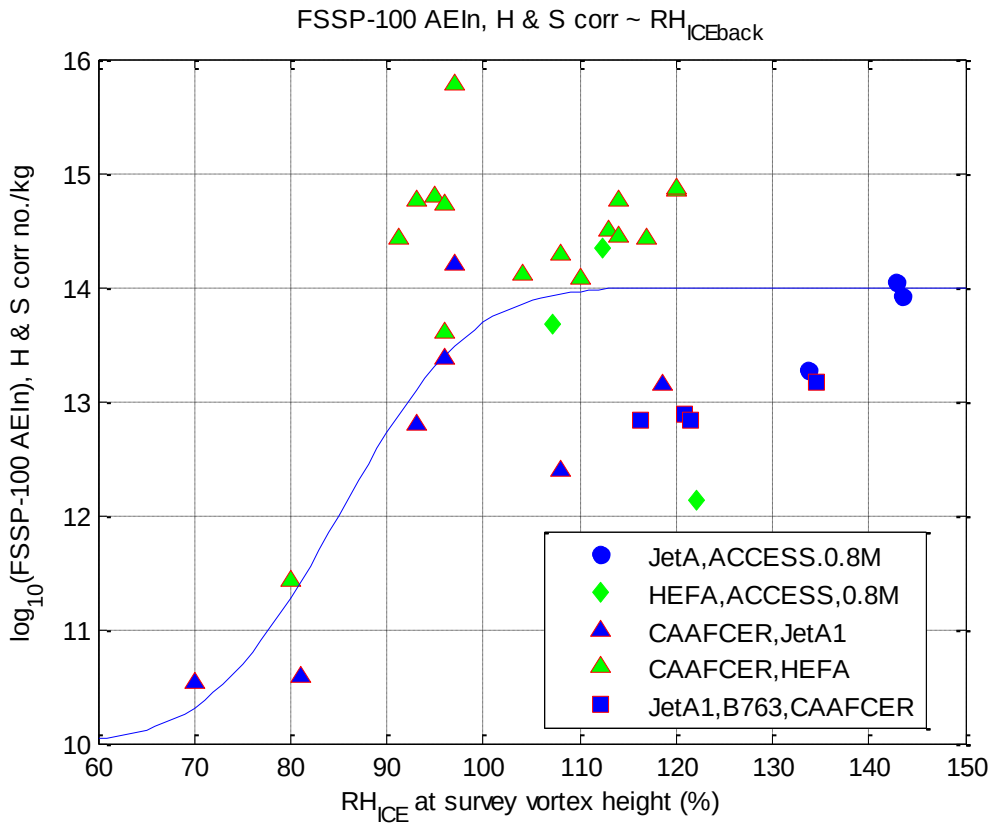

Figure 12 – plot of CAAFCER & ACCESS II NRC data of FSSP-100 AEIn against atmospheric RH_{ICECE}.

6.4 Atmospheric relative humidity lapse rate

Unlike the treatments above for T_S and RH_{ICE}, a functional relationship between contrail FSSP AEIn and $\partial RH/\partial z$ was not evident (Figure 13). Hence, a simple linear function of positive gradient (lapse rate) has been chosen. Lapse rate was observed on ACCESS II contrail data [7] to be associated with localized changes in AEIn. In that data case, the contrails were essentially confined to the TWV regions, which were descending and thus the $_{ICE}$ sublimation rate would have dependency on the TWV descent rate and RH lapse rate accordingly.

The CAAFCER contrails were UJW type, stem and crown, of 150-200 metres in depth, developed under the TWV entrainment process at formation, wherefore vortex strength is greatest. As vortex decay occurred, detrainment generally occurred with subsequent contrail development in the crown and upper-stem of the UJW. For this, a positive gradient could be expected to promote $_{ICE}$ particle growth in the crown/upper-stem of the contrail UJW. On the other hand, a negative gradient could be expected to promote $_{ICE}$ particle formation and growth in the lower stem of the UJW. Both effects, at times, have been observed in CAAFCER contrails (in particular, by the observation of low-MED location in the relevant cross-sectional segments). As mentioned earlier, UJW-crown lateral spread, including transformation to cirrocumulus, was also observed.

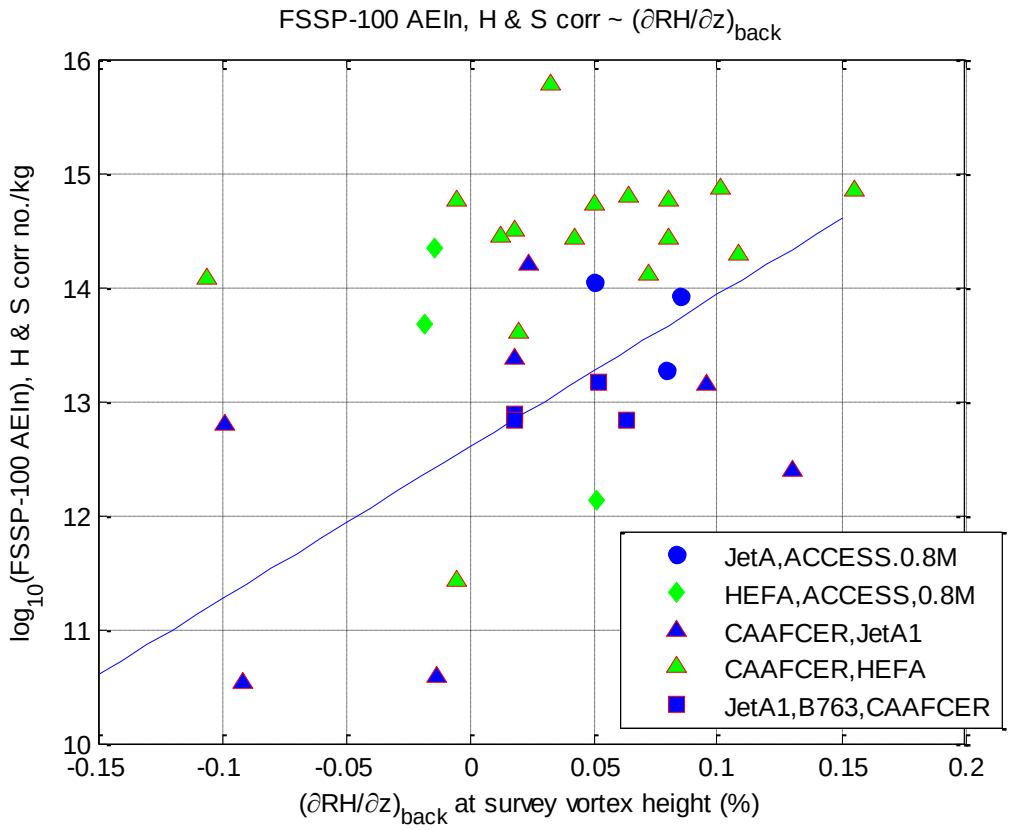

Figure 13 – plot of CAAFCER & ACCESS II NRC data of FSSP-100 AEIn against atmospheric RH lapse rate, ∂RH/∂z.

6.5 Parameterisation process – combined fuels' contrail data-set

Having assigned functional relationships for the individual effects upon contrail FSSP AEIn of the atmospheric parameters of T_S, RH_{ICE} and ∂RH/∂z, the following product-power-law relationship was used for parameter-identification:

$$Log_{10}[\text{FSSP AEIn, for both JetA1 \& HEFA}] = A(\partial RH/\partial z)^a T_S^b RH_{ICE}^c$$

For solving, the above expression was linearized by taking the logarithms of both sides, resulting in the right hand side consisting of a sum of vectors of data-point parameter values. The above equation was transformed to a linear system of column vectors by taking the logarithms of both sides. Thence, a Matlab® least squares vector identifier ('\' left-matrix divide operator) was used to identify the amplitude and exponent vector [A a b c]. In order to evenly weight the parametric influences, the assigned functional relationships were normalised, i.e. the vector [A a b c] identified for a unit value of (each log_{10}[FSSP AEIn] point) /typical(log_{10}[FSSP AEIn]). For this, log_{10}[FSSP AEIn]=15 was used. *Note:* for this identification, only CAAFCER contrails have been used.

Identified by this process, [A a b c] = [1.1934 -0.3532 0.9927 1.2497] for the combined data-set of JetA1 *and* 43% HEFA/JetA1 contrails. Coefficient and exponent values close to unity are evidence supporting the selection of respective functional relationships for individual atmospheric parameters. It is seen the identification process accepted the T_S functional relationship, weighted-up the association with RH_{ICE} and inverted the association with $\partial RH/\partial z$, from a directly proportional relationship to an inverse-asymptotic relationship. This has physical meaningfulness, given that, over the *time domain* of CAAFCER contrail ages the contrails were principally characterised by the lasting effects of wake vortex dynamics (a downward flow entrainment effect), namely ragged and lasting UJW-stem contrails.

Identifying the atmospheric relationship for the combined fuel data-sets is illustrative of the analytical process. This was essentially a 'smoothing' process for variations in atmospheric conditions and their effects upon contrail $_{ICE}$ particle number density, and for the experimental errors associated with measuring $_{ICE}$ particles, integrating and deriving AEIn. However, this did not provide a comparison for the differing effects, if any, of atmospheric properties upon contrail characteristics from different fuel types.

6.6 Parameter identification– separate fuels' contrail data sub-sets

Thus, for identifying potentially different atmospheric effects upon contrails from differing fuel types, separate identifications would be warranted for each of the fuel type contrail sub-sets. When this is conducted (using the same assigned functional relationships, selected in the earlier sections), $\log_{10}$[FSSP AEIn, JetA1 ***or*** HEFA] = $A(\partial RH/\partial z)^a T_S^b RH_{ICE}^c$, the identified coefficient-exponent vectors were [A a b c] = [1.2000 -0.9378 1.8290 1.5788] for JetA1 and [1.2183 -0.2233 0.9082 1.3214] for the HEFA-blend.

The identified vectors intimate differing atmospheric effects for differing fuels, in particular a negligible $\partial RH/\partial z$ lapse rate effect for the HEFA-blend, a lesser T_S effect, and a sharper RH_{ICE} rise (as the functional relationships are normalised, $\Im(RH_{ICE})/15 < 1$), as also observed for the 43% HEFA-blend in Figures 13, 11 and 12, respectively.

Linear regressions for each fuel data sub-set are shown in the power-law plot of Figure 14. The sublimating contrail points are seen to have provided useful pivots for the linearisations. Standard deviations of contrail data points from the linearised log-power-law were 2.5% for JetA1 and 4% for the HEFA-blend. The mean-lines of the parametric power-law identifications differ by $\pm 1\sigma$.

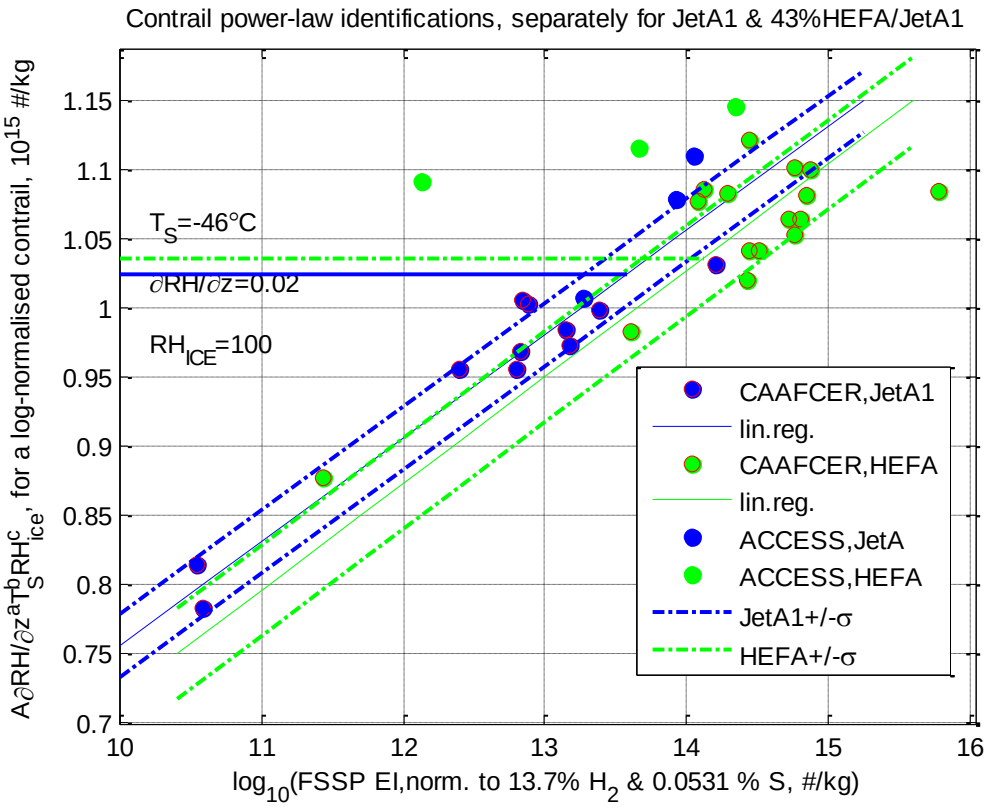

Figure 14 – plots of $A(\partial RH/\partial z)^{a}T_S^{b}RH_{ICE}^{c} = \log_{10}$[FSSP EIn], identifications for *each* of the two separate fuel type CAAFCER contrail data-sets (ACCESS data is not included in the statistical identification, merely presented for comparison).

The ACCESS II NRC data, for JetA and 50% HEFA-blend respectively, is also plotted in Figure 14, using the identified $A(\partial RH/\partial z)^{a}T_S^{b}RH_{ICE}^{c}$ for CAAFCER, for each fuel type. It is seen that the ACCESS II NRC data shares poor commonality with CAAFCER data, for each fuel type, i.e., is quite scattered in comparison (moreso, for 50% HEFA/JetA, than for JetA). The significant differences are likely engine related, but could also be associated with the differing contrail types.

As mentioned, ACCESS II contrails from the NASA DC-8 emitter were dominated by wake vortex dynamics. Nearly 100% of the contrail occurred in the vicinity of the trailing vortex cores and sublimated at approximately 15 nm contrail length. So it could be expected that the atmospheric characterisation would be somewhat different, *c.f.* to the CAAFCER contrails, which had little wake vortex-associated contrail component.

The successful linearity (within 5%) would appear to be supportive of the possibility that, for contrail production from fuels with the same normalized hydrogen and sulphur contents, the atmospheric variation effects might be more consequential than variations in aircraft types and/or individual engines of the same type. The B763 and A321 contrails quantified similarly to those

produced by the more-numerous CAAFCER A320 data – all CAAFCER data was normalized for hydrogen and sulphur contents, as discussed earlier.

Figure 14 can be used to compare FSSP AEIn for representative contrails for each fuel type, under reference atmospheric conditions, which are the mean atmospheric conditions for the two fuel types (refer to the table in section 3.1). For example, for T_S=-46°C, $\partial RH/\partial z$=0.02 and RH_{ICEce}=100%, an extrapolation upwards for JetA1 and an extrapolation downwards for HEFA-blend, for which $[A(\partial RH/\partial z)^a T_S^b RH_{ICE}^c]_{JetA1}$ = 1.024 and $[A(\partial RH/\partial z)^a T_S^b RH_{ICE}^c]_{HEFA}$ = 1.037.

The 1.3% log-normal difference is less than the standard deviations (σ) of the fuel data-sets, 2.5% and 4%, for Jet A1 and 43% HEFA respectively. Therefore, there is no statistical difference between Jet A1 and 43% HEFA contrail $_{ICE}$ particle numbers, when the AEIn *have been corrected* for differing hydrogen and sulphur contents, in accordance with $AEIn \sim [THC]^{-28}$ and $AEIn \sim [S]^{0.55}$.

For the contrail sub-sets, using separate identifications for the differing fuels, the plots of contrail $A(\partial RH/\partial z)^a T_S^b RH_{ICE}^c$ for encountered atmospheric conditions against contrail age are shown in Figure 15.

In this case, actual atmospheric conditions have been used for each contrail data-point. Thus, the use of the formulations represents a data-smoothing process, accounting for experimental variations of measurement. So the difference between JetA1 and HEFA-blend contrails, the latter showing *c.*15% log-normal more $_{ICE}$ particles, in part is due to the more conducive atmospheric conditions for contrail formation, *i.e.* colder, higher RH_{ICE} of the higher altitudes flown with the HEFA-blend.

It is seen (Figure 15) that, for the longest CAAFCER contrail on the 43% HEFA/JetA1 blend, the 'smoothed' $_{ICE}$ particle AEIn was nearly constant from 1 to 7 minutes age, rising by 1% and falling by 2%.

7.0 Contrail AEIm parameterisation, atmospheric properties

The same approach was taken for the atmospheric parameterisation of contrail $_{ICE}$-mass apparent emission index, AEIm, for $_{ICE}$ particles larger than 0.5 µm in size. The same normalisation factors for THC and S content were applied, as for $_{ICE}$ particle AEIn.

For the contrail $_{ICE}$ particle spectra (such as that of Figure 4), AEIm has been determined by volumetric integration, under the assumption of 100% sphericity of contrail $_{ICE}$ particles. For a contrail of 7 minutes age (*c.*50 nm length), this assumption is likely violated. Thus, AEIm as determined, provides a guideline only, to $_{ICE}$-mass for particles sized $\geq$ 0.5 µm. Parametric plots of AEIm against T_S, $\partial RH/\partial z$ and RH_{ICE} are presented in Figure 16. If anything, there is less variation of AEIm with atmospheric parameters. Nevertheless, the same form of functional relationships was used for power-law identification, although T_S was shifted to the left 3°C.

The product power-law $[\text{FSSP AEIm}]_{JetA1\ or\ HEFA\text{-}blend} = [A(\partial RH/\partial z)^a T_S^b RH_{ICE}^c]$, was used as before. Identifications resulted in the vector of values [A a b c] = [0.8158 -1.1639 1.9459 1.7010] for JetA1, and [0.9543 0.1066 -0.2338 1.0521] for the 43% HEFA-blend.

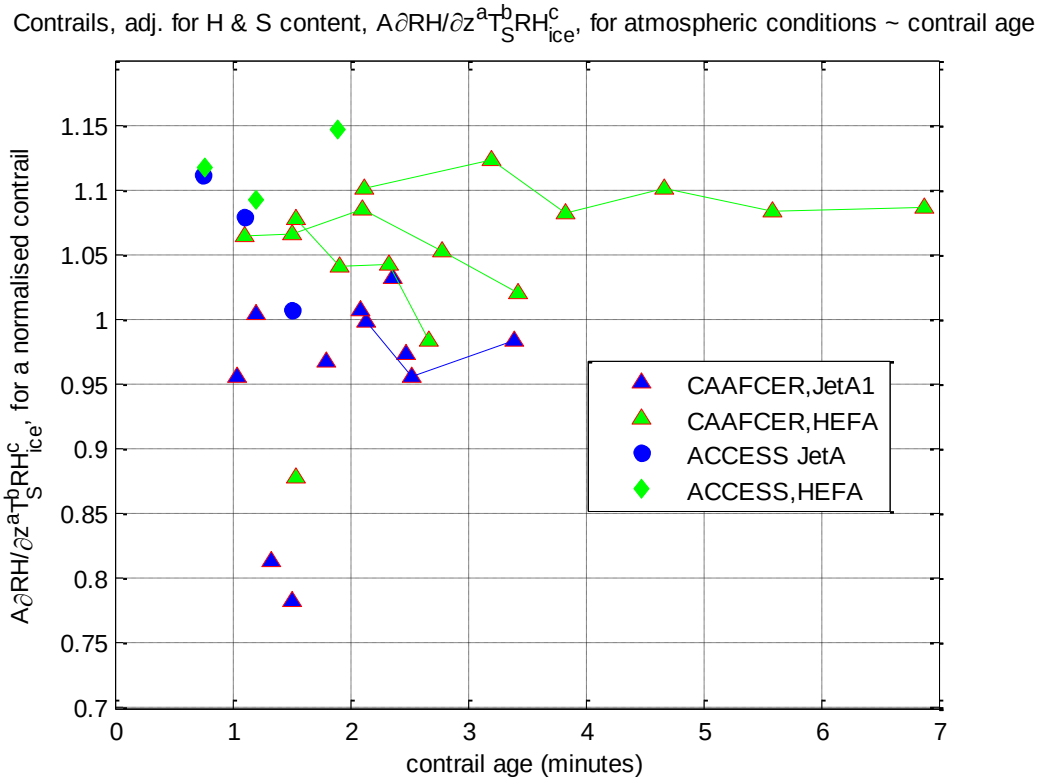

Figure 15 – plot of $A(\partial RH/\partial z)^a T_S^b RH_{ICE}^c$ identified separately for each of the two fuel types, against contrail cross-section data-point age.

The identifications are shown in Figure 17, for the two fuel types. Also shown are +2σ (i.e. 95% confidence) lines. It is seen that the mean-lines for each fuel-type are separated by >2σ. This indicates that there is a statistical difference in $_{ICE}$-mass (for spherical integration), with the 43% HEFA-blend contrails having less >0.5µm particle size $_{ICE}$-mass.

Using the identification for the reference atmospheric conditions as before (T_S = -46°C, $\partial RH/\partial z$ = 0.02 %/m and RH_{ICE} = 100%), the contrail normalised (by 10^8 µg/kg) $_{ICE}$ masses were 1.155 and 1.036, for JetA1 and 43% HEFA/JetA1, respectively. In quantity terms, these figures amount to, for JetA1, $10^{(8*1.155)}$ µg/kg = 1.74 kg/kg, and for 43% HEFA/JetA1, $10^{(8*1.036)}$ µg/kg = 0.19 kg/kg, implying an 89% reduction in $_{ICE}$-mass for the HEFA-blend, *c.f.* JetA1, a large and possibly excessive difference, *e.g.*, subject to error induced by the sphericity assumption, for example. This would imply, for the same AEIn after THC and S adjustments to reference values, an $_{ICE}$ particle

size comparison of 43% HEFA being $(0.19/1.74)^{(1/3)} = 0.48$, or half that for JetA1, or a 52% reduction in mean $_{ICE}$ particle size for the 43% HEFA-blend. The development of sphericity would make this size comparison quite inaccurate.

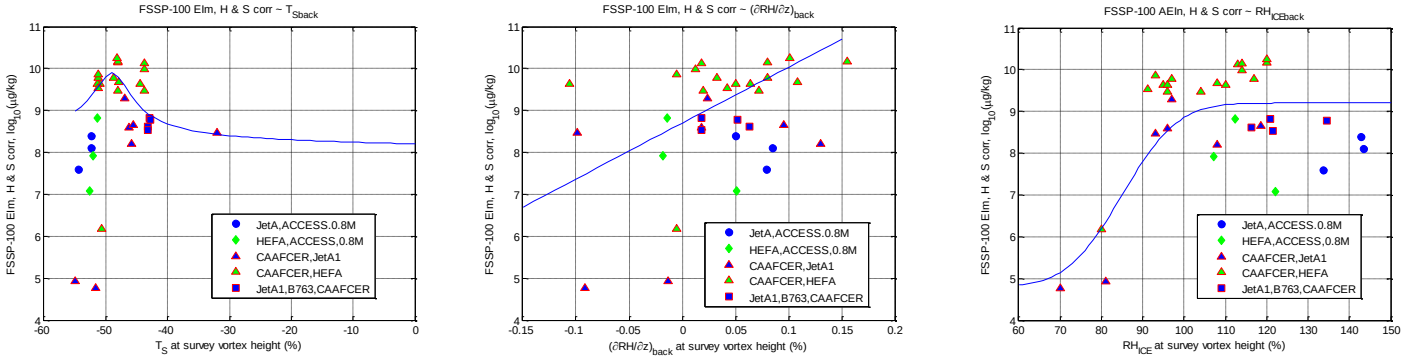

Figure 16 – plots of CAAFCER & ACCESS II NRC data of FSSP-100 AEIm against atmospheric temperature T_S, RH lapse rate $\partial RH/\partial z$ and relative humidity over $_{ICE}$ RH_{ICECE}.

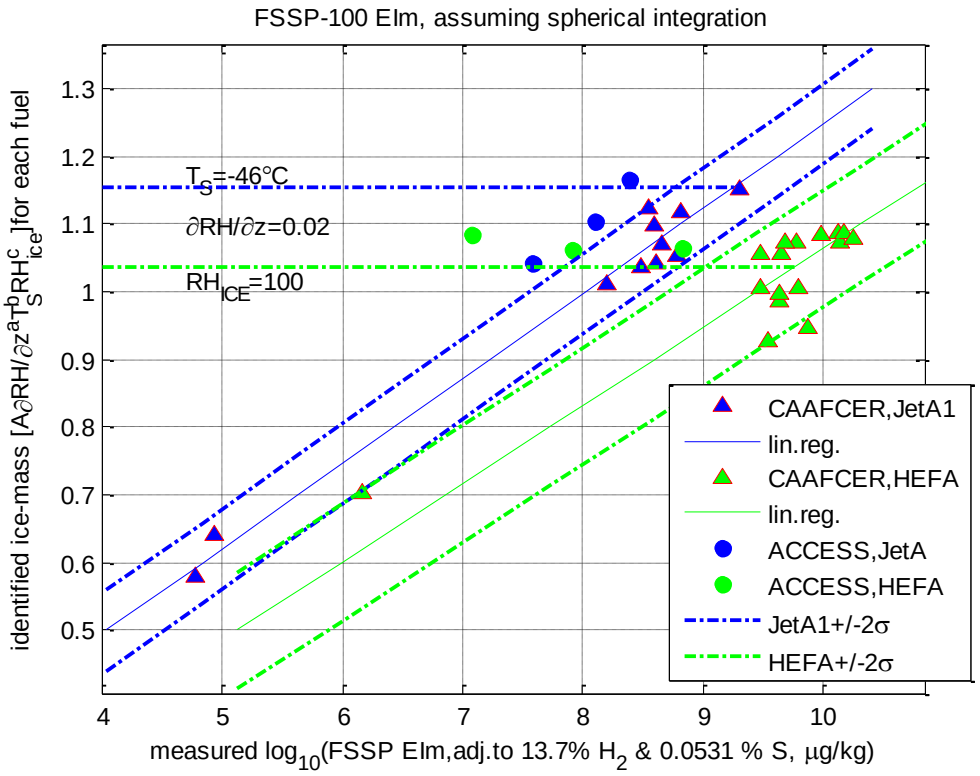

Figure 17 – plots of log-normal (by 10^8 µg/kg) $A(\partial RH/\partial z)^a T_S{}^b RH_{ICE}{}^c = \log_{10}$[FSSP AEIm], identifications of contrail spherically-assumed $_{ICE}$-mass, for *each* of the two separate fuel type contrails.

The $_{ICE}$-mass relationship with contrail age is shown in Figure 18, for the encountered atmospheric conditions and measured FSSP AEIm (spherically-integrated), adjusted to reference hydrogen and sulphur contents, and smoothed for experimental measurement errors, using the above

[$A(\partial RH/\partial z)^a T_S^b RH_{ICE}^c$] identifications. Sequential AEIm data-points for an individual contrail are linked by lines, in Figure 18.

It is seen that the longest biofuel contrail has slowly-decaying $_{ICE}$-mass, in a reasonably smooth manner, which might be evidence of sublimation with the maintenance of sphericity (as opposed to asphericity, which would likely manifest sequential variability in EIm due to variable measurement of apparent particle size in crystalline conditions). Evidence of sphericity could possibly be observed also in the $_{ICE}$ particle spectra from the FSSP-100. Spectra have been extracted from the more homogenous parts of the contrail (defined as where the probe activity count is reasonably constant).

These spectra are shown in Figure 19, for various contrail lengths from 27 to 83 km. Retention of sphericity could be expected to yield skewed-Gaussian spectra (showing regular changes in adjacent bin numbers of $_{ICE}$ particles), like that observed in the spectra of Figure 4. It is seen that the spectra in Figure 19, for contrail lengths from 27-83 nm, show significant irregularities between adjacent bins, possibly evidence of asphericity in the form of crystalline $_{ICE}$ particles – but the degree of irregularity does not change greatly over the contrail length range (for homogenous sections of contrail). As mentioned earlier, the growth of crystalline, aspherical ice particles will substantially render spherically-derived ice-mass estimations inaccurate.

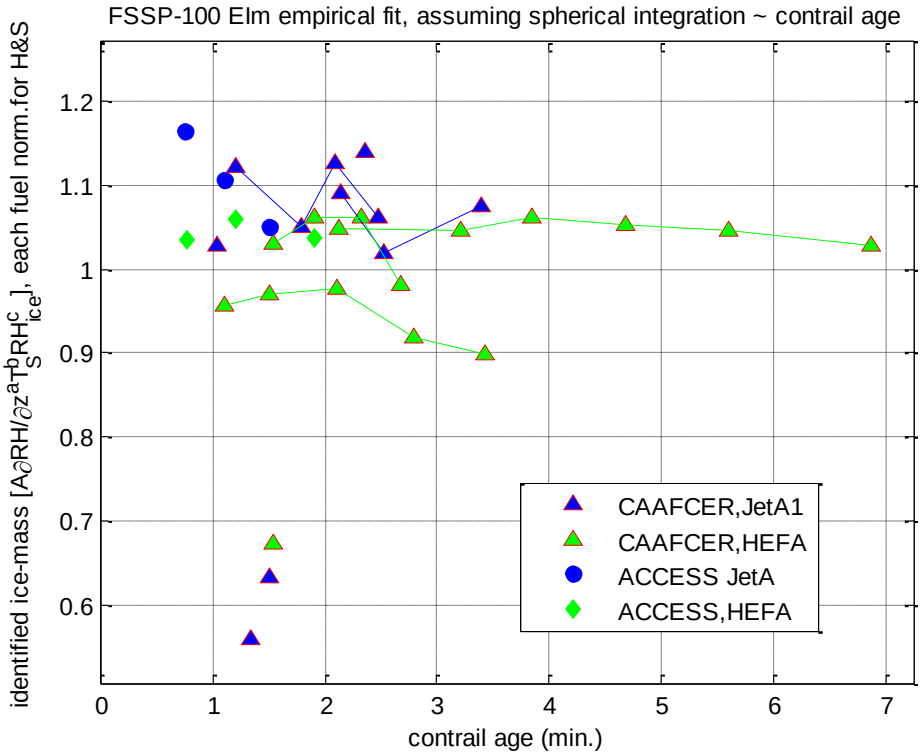

Figure 18 – plot of ice-mass $A(\partial RH/\partial z)^a T_S^b RH_{ICE}^c$ identified separately for each of the two fuel types, against contrail cross-section data-point age (assumes spherical integration and ρ=1000 kgm^{-3}.

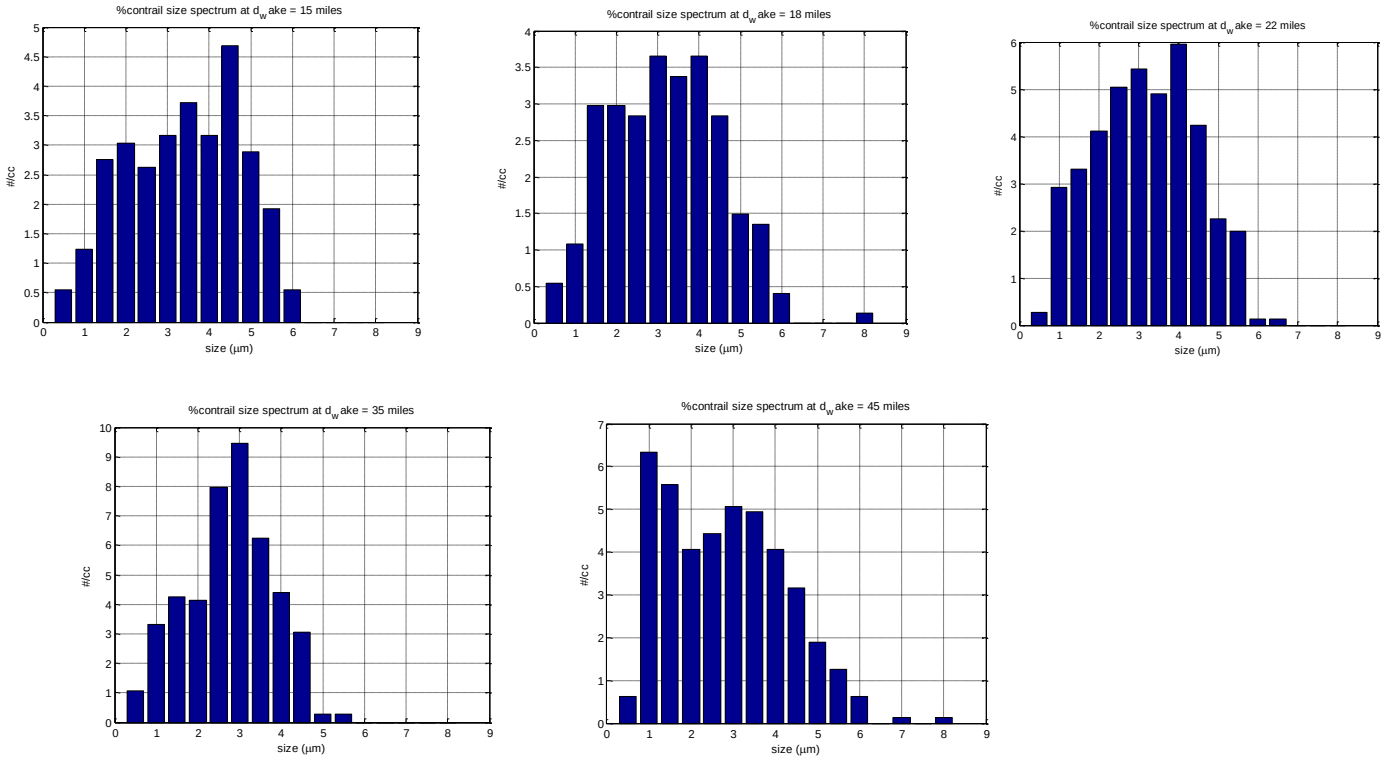

Figure 19 – contrail $_{ICE}$ particle spectra, FSSP-100, in homogenous sections of the contrail, at various contrail lengths:- *top, left to right*, 15 nm, 18 nm, 22 nm; *bottom, left to right*, 35 nm, 45 nm.

8.0 MED parameterization with atmospheric properties

The contrail FSSP-100 measured $_{ICE}$ particle sizing spectra have been used to derive, for each data-point spectrum (gathered at 10 Hz), the $_{ICE}$ particle Median Effective Diameter (MED), defined as the spherical particle diameter equivalent to the 50th percentile of the FSSP-100 cumulative $_{ICE}$-volume of that spectrum. For this, $_{ICE}$ particle sphericity is assumed (as it has been, likewise, for AEIm derivation; discussed in the preceding section; Figure 18 refers to this discussion).

Thereafter, concatenated contrail cross-sectional contour plots of MED distributions have been derived. A typical plot was presented in Figure 4. Further plots are presented in Figure 20(a), (b), several plots at increasing contrail length for a 43% HEFA blend and a Jet A1 case. It is seen $_{ICE}$ particle size growth occurred in varying regions, UJW or TWV. Background atmospheric RH lapse rate and its interaction with the TWV are significant parameters of dependency in the growth of $_{ICE}$ particle size. As seen in Figures 4 and 20, there are varieties of MED values, dependent upon the regime of the contrail cross-section. In particular, smaller MED values were in the TWV regime for this particular plot, indicating that $_{ICE}$ particle size growth has slowed-down or reversed (*i.e.*, sublimation onset has occurred in the TWV regime), whereas size growth might still be occurring in the UJW regime.

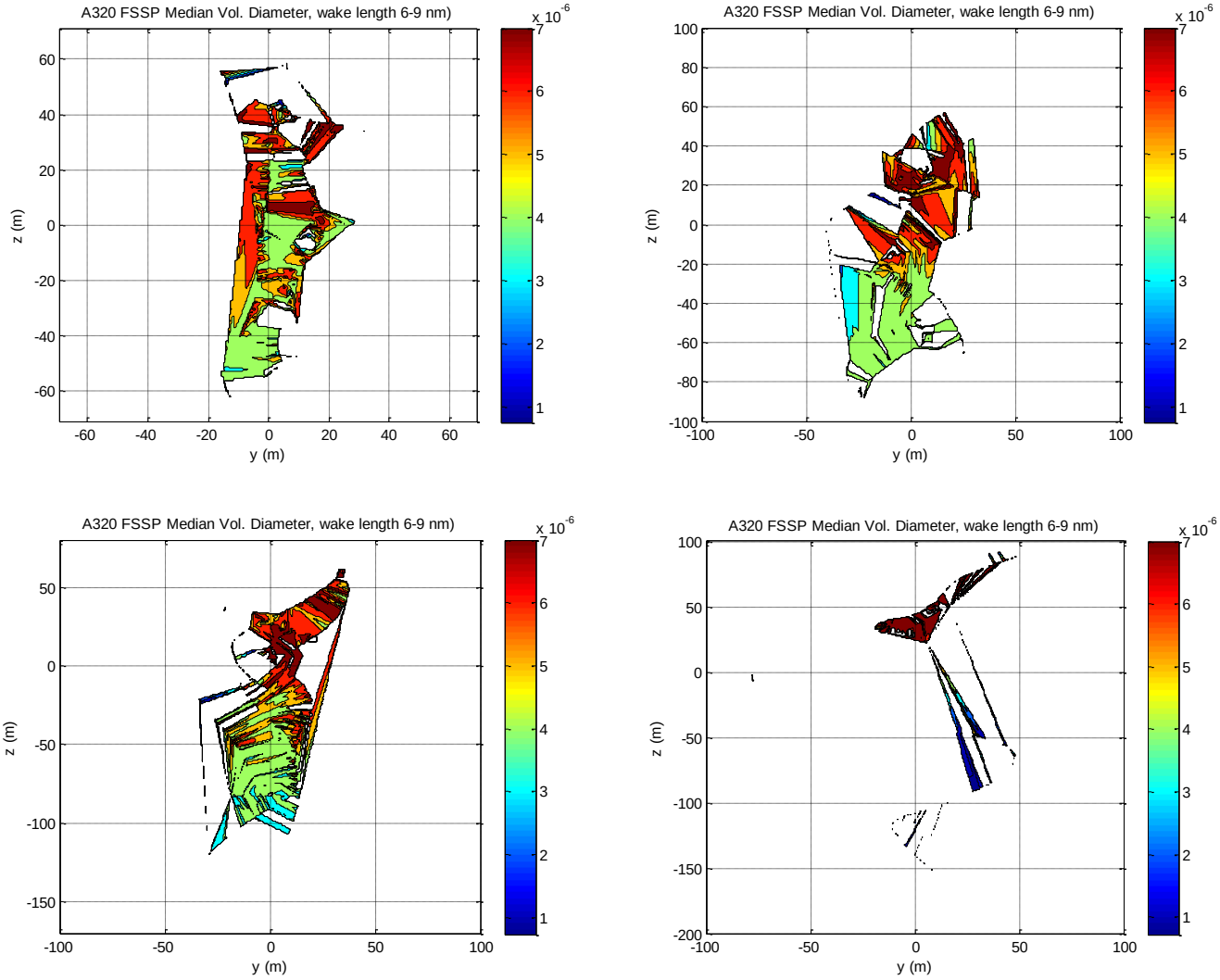

Figure 20(a) – contour cross-plane plots of contrail FSSP-100 ice particle spectral MED (43% HEFA contrail, 3rd May 2017), showing size growth in the UJW and sublimation in the TWV regions over increasing contrail length:- *top, left to right*, 8 nm, 12 nm; *bottom, left to right*, 15 nm, 18 nm.

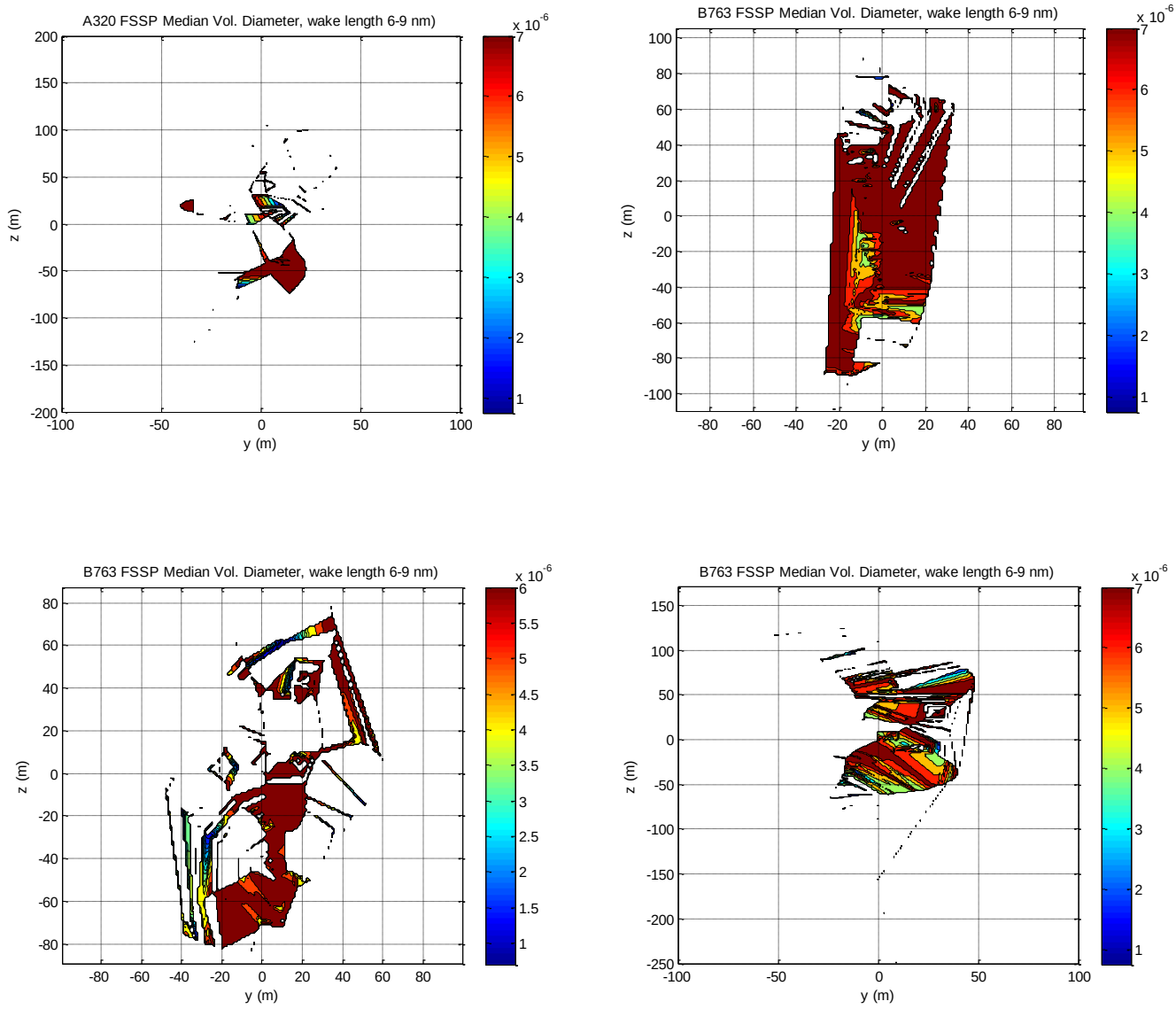

Figure 20(b) – contour cross-plane plots of contrail FSSP-100 ice particle spectral MED (Jet A1 contrail, 3rd May 2017), showing size growth in the UJW and sublimation in the TWV regions over increasing contrail length:- *top, left to right*, 123nm, 16 nm; *bottom, left to right*, 19 nm, 22 nm.

Thus, MED could be expected to also vary with influential atmospheric parameters, perhaps similarly to AEIn and AEIm. For this exploration, with due regard to the cross-sectional variation in MED as observed in Figures 4, 20(a) and (b), a statistical representation of the various MED values distributed in a single cross-section is required (as opposed to AEIn and AEIm, which are both [y z] spatial integrations). For this statistical representation, both median and mean values of MED (in a *single* cross-sectional plot) have been considered, and the median value has been subsequently used for atmospheric parametric analysis.

Furthermore, no corrections to MED are warranted, nor have been applied, to the MED values derived from size spectra measured by the FSSP-100.

The atmospheric parametric cross-plots of median MED, for all measured contrails, are shown in Figure 21. Also shown is a plot the development of cross-sectional median MED with contrail age. It shows that ACCESS II contrails had small $_{ICE}$ particles due to sublimation by 26 km length (median MED values were of the order of 1 µm, which implies minimum size resolution for the FSSP-100). CAAFCER contrails had median contrail cross-sectional MED values in the range 2-9 µm, with some high-rate spatiotemporal changes to median MED, as high 2.2 µm (from 5 to 7.2 µm) in 1/3 minute and an associated spatial change of 4.6 km along-track.

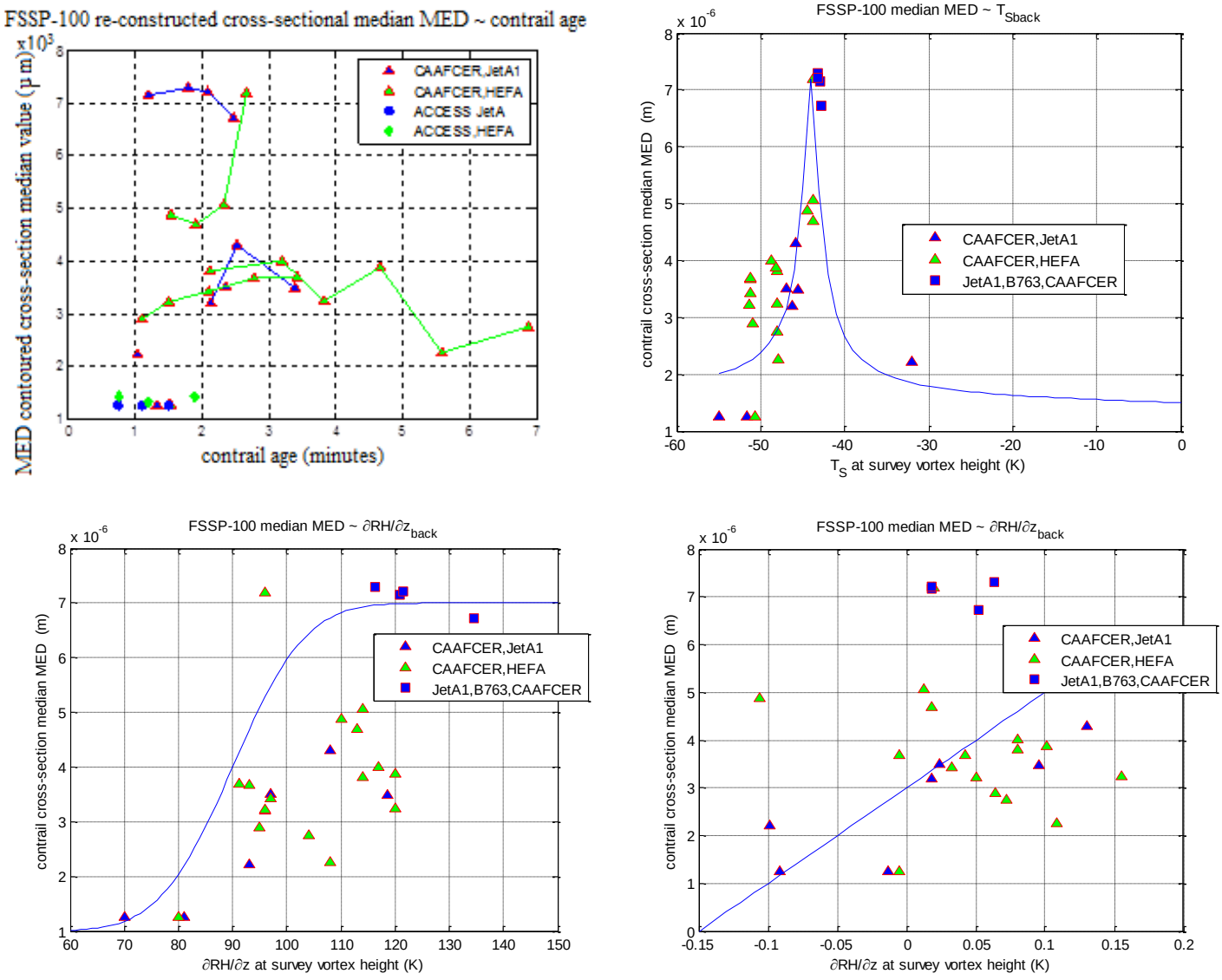

Figure 21 – plots of median MED for each contrail cross-sections, plotted against *top left*, contrail age (and along-track spatial changes) and atmospheric parameters, *top right*, T_S, *bottom left*, RH_{ICEce}, *bottom right*, ∂RH/∂z.

For the variations of median MED with atmospheric parameters (i.e., with T_S, RH_{ICE} and ∂RH/∂z), the same functional forms have been used as for AEIn and AEIm, as shown in Figure 22. The

least-squares-error identification of the parametric power-law for each of the two fuel-types is shown in Figure 22. For the reference atmospheric conditions, a T_S = -46°C, RH_{ICE} = 100% and $\partial RH/\partial z$ = 0.02 %/m, the identification indicates a median MED of the order of 4 µm and a reduction in 43% HEFA $_{ICE}$ particle size of approximately 10%, *c.f.* Jet A1, implying a reduction of median $_{ICE}$-mass of 27%.

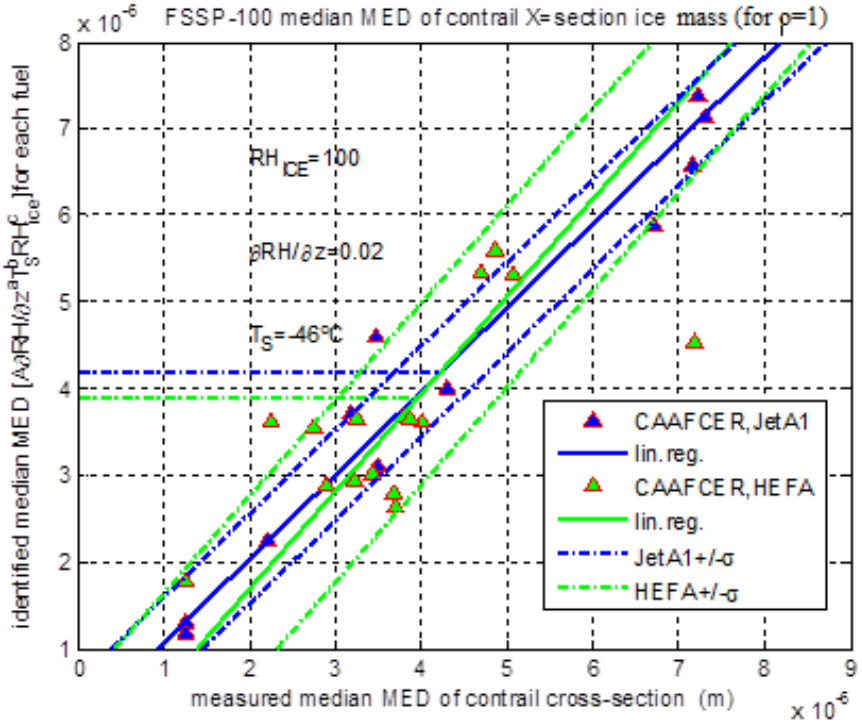

Figure 22 – plots of identified power-law parametric variations of contrail cross-section median MED with atmospheric properties, for the two fuel types used on CAAFCER,

9.0 Summary

Under GARDN project CAAFCER, research flights were conducted into the fuel effects upon contrail development, for JetA1 and for a blend of 43% HEFA/JetA1. CAAFCER was conducted on a number of aircraft, including different engine models. Contrails were formed under jet-stream influence, in the St Lawrence Seaway UTLS atmosphere. In broad type, the contrails generated in these atmospheric conditions, by Air Canada A320 (CFM56-5B4/P engines), A321 (CFM56-5B3/P engines) and B763 (CF6-80C2 B1F/B6F engines) generators were UJW dominated, unlike ACCESS II contrails, which were TWV dominated.

Contrail analysis has been conducted, under the premise of assessing fuel property and atmospheric effects for a lumped data-set of contrails for differing aircraft and engine types and serial numbers, in order to assess whether *or not* there was commonality of effects. In this regard,

ACCESS II data has also been considered. The ACCESS II data was all obtained from an individual aircraft, a DC-8 with four CFM56-2-C1 engines.

Individual wing-tank fuel sample testing was conducted. This was satisfactorily accurate for the arrival, JetA1-fueled aircraft. However, for the departing 43% HEFA-fueled aircraft, contamination occurred from residual, undrainable JetA1 remaining in the tank sumps prior to refueling with 43% HEFA. So, for 43% HEFA fuel properties, the composition tests of unblended JetA1, HEFA and blended 43% HEFA/JetA1 were all considered, particularly in relation to hydrogen content. Finally, 43% HEFA hydrogen content was derived by estimation, in accordance with ASTM D-3343. For all fuel samples, nuclear magnetic resonance determination of hydrogen content of 43% HEFA samples showed good agreement with the ASTM D-3343 methodology, with a standard deviation of 0.07%.

CAAFCER tested hydrogen content for JetA1 samples varied from 13.6 to 13.8%. For 43% HEFA, ASTM D-3343 estimated hydrogen content, adjusted for tank residual fuel, was 14.56%. These are close to the ACCESS II hydrogen content of 13.7% for Jet A and 14.5% for 50% HEFA. ACCESS II Jet A and 50% HEFA contrail data showed strong reductions of AEIn (>0.5µm) with increasing hydrogen content, similar to that of nvPM AEIm data from ground test cell measurements.

For comparison between fuels and projects (to assess potential differences between engine, aircraft and contrail type effects), CAAFCER contrail FSSP AEIn was adjusted to reference hydrogen content (13.74%), using an experimental-fit exponent of -28, for each of the two fuel types. Using this exponent, the hydrogen content uncertainty (0.07%) equates to an AEIn uncertainty of $(1\pm 0.07/13.74)^{-28} = \pm 15\%$ in AEIn.

Adjusted CAAFCER AEIn, showed slight variations with fuel sulphur content, exhibiting a direct relationship, with an exponent, which was approximately one-third that of the vPM EIn exponent measured for volatile particulates on the Aerodyne/NASA sulphur flight experiment. For comparison between fuels and projects (to assess potential differences between engine, aircraft and contrail type effects), CAAFCER contrail AEIn data was adjusted to reference sulphur content (0.052%), using an exponent of 0.55, for each of the two fuel types.

The adjusted AEIn (to reference hydrogen and sulphur content) data was then parameterised for variation of the atmospheric parameters of air temperature, relative humidity over $_{ICE}$ and RH lapse rate with height. Shape functions were used for associations between AEIn and each parameter – resonance, error and linear functions, respectively. The functions were lumped in a product power-law, $A\Im(T_S)^a\Im(RH_{ICE})^b\Im(\partial RH/\partial z)^c$, and identification conducted for each fuel type, using a maximum-likelihood estimator.

When normalised to reference H and S content and so analysed, there was no statistical difference between Jet A1 and 43% HEFA fuels, for reference atmospheric conditions (the mean of

CAAFCER atmospheric conditions, namely air temperature -46°C, 100% RH_{ICE} and RH lapse rate of 0.02%/m), implying fuel properties normalization effectively provided equivalence of AEIn between fuels.

The spherically-integrated contrail $_{ICE}$-mass AEIm (for >0.5 μm) showed a statistically-significant reduction in $_{ICE}$ volume for 43% HEFA-blend contrails, compared to Jet A1.

The two results, comparisons for AEIn and AEIm, are consistent with the $_{ICE}$ particle size measurements being smaller for 43% HEFA-blend *c.f.* JetA1. Statistical analysis of FSSP-100 data, in the form of the median MED sizing of $_{ICE}$ particles, showed a reduction in size, for 43% HEFA, but an incremental value less than a standard deviation of the data-sets.

10.0 Conclusions

For the jet fuels used on CAAFCER, 43% HEFA/Jet A1 and JetA1, contrail $_{ICE}$ particle number AEIn (>0.5 μm size) correlated inversely with fuel hydrogen content, and, to a much lesser extent, directly with fuel sulphur content. This was demonstrated for flight data: lumped atmospheric effects upon contrail AEIn were not different for fuel type, Jet A1 or 43% HEFA blend, when corrected to the same hydrogen and sulphur content. Biofuels have increased hydrogen content and reduced sulphur content, and thus, given the correlation, could be expected to generate fewer contrail $_{ICE}$ particles.

On the other hand, the contrail $_{ICE}$ spherical volume, AEIm, differed between fuel types. It was significantly less for 43% HEFA, *c.f.* Jet A1, although the development of aspherical $_{ICE}$ crystalline shapes, could have contributed to the over-estimation of $_{ICE}$-volume difference. The median effective $_{ICE}$ particle size comparison supported this difference between fuel types, *albeit* to a lesser extent. The sizes for 43% HEFA contrails were approximately 10% smaller than that for Jet A1 contrails.

These findings support the desirability of undertaking further research flights, with fuels having the reasonably widest range of hydrogen and sulphur content and using the same engine serial numbers, throughout. Finally, the employment of contrail optical-effect sensors on the CT-133 through the course of such additional flight research would enable the contrail differences from biofuels to be translated to optical effects, thence to quantify the global-warming radiative forcing reduction potential from biofuels.

11.0 References

1. Environment Branch of the International Civil Aviation Organisation, "ICAO Environmental Report 2016, Aviation and Climate Change."
2. Karcher, B. and Voigt, C., "Susceptibility of contrail $_{ICE}$ particle numbers to aircraft and particle emissions," Geophysical Research Letters, 10.01002/2017GL074949, August 2017.
3. Chan, T.W., Canteenwalla, P., Chishty, W. W., "GT2017-63131, Characterisation of Fuel Composition and Altitude Impact on Gaseous and Particle Emissions from a Turbojet Engine," Proceedings of ASME Turbo Expo 2017, GT2017, 26-30 June 2017, Charlotte, NC, USA.
4. Moore, R.H. *et al*, "Biofuel blending reduces particle emissions from aircraft engines at cruise conditions," Nature, doi:10.1038/nature21420, 2017.
5. Miake-Lye, R. C., *et al*, "SO_x oxidation and volatile aerosol in aircraft exhaust plumes depend on fuel sulphur content, G.R.L., Vol.25, No.19, pp 1670-1680, 15 May 1998.
6. Brown, A.P., Bastian, M., Pryor, M., Talgoy, P., "NRC CT-133 ACCESS II DATA ANALYSIS:- GASEOUS, AEROSOL AND CONTRAIL CHARACTERISTICS**,"** Flight Research Laboratory, NRC IFAR NASA ACCESS II Data Workshop, Kissimmee, FL, 9th January 2015
7. Brown, A.P., Bastian, M., Alavi, S., Wasey, M., "FLIGHT RESEARCH REPORT:- PROJECTS AEAFFR, CAAFER AND NASA ACCESS II JET TRANSPORT EMISSIONS MEASUREMENTS,' NRC LTR-FRL-2015-0054, March 2015.
8. Poitras, P., "NRC Biofuel Flight Program Sample Testing," QETE 19100-1 (H001917), 21 July 2017, Quality Engineering Test Establishment, DND.
9. P. Jeßberger, C. Voigt, U. Schumann, I. Sölch, H. Schlager, S. Kaufmann, A. Petzold1, D. Schäuble, and J.-F. Gayet, "Aircraft type influence on contrail properties," Atmos. Chem. Phys., 13, 11965–11984, 2013 www.atmos-chem-phys.net/13/11965/2013/ doi:10.5194/acp-13-11965-2013.
10. Karcher, B., "The importance of contrail $_{ICE}$ formation for mitigating the climate impact of aviation," Journal of Geophysical Research: Atmospheres, 10.1002/2015JD024696, 2016, *pp* 3497-3505..
11. "CAAFCER Fuel Traceability Report," Sky NRG.
12. Poitras, P., "ASTM D-3343-16 Method of Hydrogen Content Estimation Spreadsheet," Quality Engineering Test Establishment (QETE), DND.
13. Brown A.P., Bastian, M., Femia, F., Salib, M.,Ghatala, F., Olfert, J.,Beunis, R., Valk, M., "GARDN CAAFCER Biofuel Contrail Operations Report," LR-FRL-2018-0013, NRC Canada, February 2018.